Atmos. Chem. Phys. Discuss., doi:10.5194/acp-2016-60, 2016
Manuscript under review for journal Atmos. Chem. Phys.
Published: 10 February 2016


Atmospheric Chemistry and Physics Discussions

# In-situ observations of the isotopic composition of methane at the Cabauw tall tower site

Thomas Röckmann[1,*], Simon Eyer[2,*], Carina van der Veen[1], Maria E. Popa[1], Béla Tuzson[2], Guillaume Monteil[1,3], Sander Houweling[1], Eliza Harris[2], Dominik Brunner[2], Hubertus Fischer[7], Giulia Zazzeri[4], David Lowry[4], Euan G. Nisbet[4], Willi A. Brand[5], Jaroslav M. Necki[6], Lukas Emmenegger[2] and Joachim Mohn[2]

[1] Utrecht University (UU), Institute for Marine and Atmospheric Research Utrecht (IMAU), The Netherlands

[2] Empa, Laboratory for Air Pollution / Environmental Technology, Dübendorf, Switzerland

[3] now at Department of Physical Geography and Ecosystem Science, Lund University, Lund, Sweden

[4] Royal Holloway University of London (RHUL), Department of Earth Sciences, Egham, UK

[5] Max-Planck-Institute (MPI) for Biogeochemistry, Jena, Germany

[6] Environmental Physics Group, Faculty of Physics and Applied Computer Science, AGH University of Science and Technology, Krakow, Poland

[7] University of Bern, Climate and Environmental Physics, Bern, Switzerland

*These authors contributed equally to this work

Atmos. Chem. Phys. Discuss., doi:10.5194/acp-2016-60, 2016
Manuscript under review for journal Atmos. Chem. Phys.
Published: 10 February 2016


Atmospheric Chemistry and Physics Discussions

**Abstract**

High precision analyses of the isotopic composition of methane in ambient air can potentially be used to discriminate between different source categories. Due to the complexity of isotope ratio measurements, such analyses have generally been performed in the laboratory on air samples collected in the field. This poses a limitation on the temporal resolution at which the isotopic composition can be monitored with reasonable logistical effort. Here we present the performance of a dual isotope ratio mass spectrometric system (IRMS) and a quantum cascade laser absorption spectroscopy (QCLAS) based technique for in-situ analysis of the isotopic composition of methane under field conditions. Both systems were deployed at the Cabauw experimental site for atmospheric research (CESAR) in the Netherlands and performed in-situ, high-frequency (approx. hourly) measurements for a period of more than 5 months. The IRMS and QCLAS instruments were in excellent agreement with a slight systematic offset of +(0.05 ± 0.03) ‰ for $\delta^{13}C$ and –(3.6 ± 0.4) ‰ for δD. This was corrected for, yielding a combined dataset with more than 2500 measurements of both $\delta^{13}C$ and δD. The high precision and temporal resolution dataset does not only reveal the overwhelming contribution of isotopically depleted agricultural $CH_4$ emissions from ruminants at the Cabauw site, but also allows the identification of specific events with elevated contributions from more enriched sources such as natural gas and landfills. The final dataset was compared to model calculations using the global model TM5 and the mesoscale model FLEXPART-COSMO. The results of both models agree better with the measurements when the TNO-MACC emission inventory is used in the models than when the EDGAR inventory is used. This suggests that high-resolution isotope measurements have the potential to further constrain the methane budget, when they are performed at multiple sites that are representative for the entire European domain.

Atmos. Chem. Phys. Discuss., doi:10.5194/acp-2016-60, 2016
Manuscript under review for journal Atmos. Chem. Phys.
Published: 10 February 2016


Atmospheric Chemistry and Physics Discussions

## 1. Introduction

The global increase of the important greenhouse gas methane in the atmosphere since the beginning of the industrial period is very well established (Dlugokencky et al., 2009; Dlugokencky et al., 1996; Dlugokencky et al., 1998; Etheridge et al., 1998; Khalil et al., 2007; Loulergue et al., 2008; MacFarling Meure et al., 2006; Rasmussen and Khalil, 1981; Spahni et al., 2005). The existing $CH_4$ mole fraction measurement data enable accurate assessment of the source-sink imbalance through time, and together with the estimated total sink strength, they allow for a top-down constraint on the global source of methane to the atmosphere (Bergamaschi et al., 2013; Houweling et al., 2014). Bottom-up estimates of the global methane budget carry much larger uncertainties, which are inherent to the assumptions made in the extrapolation of local scale measurements to larger scales (Bruhwiler et al., 2014; Kirschke et al., 2013; Nisbet et al., 2014). The advantage of bottom-up estimates is, however, the possibility to distinguish different sources and to link observations to process-level understanding of the emissions.

An independent approach for distinguishing between source categories of $CH_4$ is the analysis of its isotopic composition, which is strongly linked to the source/sink processes. This is particularly true for methane from biogenic, thermogenic and pyrogenic sources (Gros et al., 2004; Houweling et al., 2008; Quay et al., 1999; Sapart et al., 2012). A more detailed differentiation within one source category, e.g. biogenic $CH_4$, for emissions from wetlands, ruminants, rice paddies or termites, however, is complicated because of the overlap of the respective isotopic source signatures. Further complications arise because individual source signatures can show pronounced dependence on environmental parameters and metabolized substrates (Kawagucci et al., 2014; Klevenhusen et al., 2010). In addition to the source contributions, the sink processes (mainly chemical removal by the hydroxyl radical (OH), but also soil deposition and stratospheric loss) also affect the isotopic composition of atmospheric methane (Brenninkmeijer et al., 1995; Röckmann et al., 2011; Saueressig et al., 1996; Saueressig et al., 2001; Snover and Quay, 2000). Nevertheless, over the past decades, numerous studies have shown the potential of isotope measurements to identify individual source categories from isotope

Atmos. Chem. Phys. Discuss., doi:10.5194/acp-2016-60, 2016
Manuscript under review for journal Atmos. Chem. Phys.
Published: 10 February 2016


Atmospheric Chemistry and Physics Discussions

observations (Beck et al., 2012; Lassey et al., 1993; Tarasova et al., 2006; Umezawa et al., 2012b; Zazzeri et al., 2015) and to constrain budgets (Ferretti et al., 2005; Fischer et al., 2008; Houweling et al., 2008; Lassey et al., 2000; Lowe et al., 1994; Sapart et al., 2012; Umezawa et al., 2012a).

$CH_4$ mole fractions $\chi(CH_4)$ are reported in nmol/mol = $10^{-9}$ and µmol/mol = $10^{-6}$. The isotopic composition is commonly reported in δ notation, where δ quantifies the relative deviation of an isotope ratio ($^{13}R$ = $^{13}C/^{12}C$ for carbon isotopes and $^{2}R$ = $^{2}H/^{1}H$, abbreviated as D/H, for hydrogen isotopes) in a sample from a standard ratio. The international standard for reporting $\delta(^{13}C, CH_4)$ values is Vienna PeeDeeBelemnite (VPDB, $^{13}R_{VPDB}$ = 0.0112372 (Craig, 1957)) and for $\delta(D, CH_4)$ it is Vienna Standard Mean Ocean Water (VSMOW, $^{2}R_{VSMOW}$ = 0.0020052 (Baertschi, 1976)). $\delta(^{13}C, CH_4)$ and $\delta(D, CH_4)$ are abbreviated as $\delta^{13}C$ and δD in the following, and given in per mill (‰). For interpretation of global or continental scale atmospheric data the expert group of the WMO/IAEA has set a scientifically desirable level of compatibility of 2 nmol/mol, 0.02 ‰ and 1 ‰ for $CH_4$ fraction, $\delta^{13}C$ and $\delta D$, respectively (WMO, 2014). For regionally focused studies with large local fluxes, extended compatibility goals of 5 nmol/mol, 0.2 ‰ and 5 ‰ for $\chi(CH_4)$, $\delta^{13}C$ and $\delta D$ were defined.

Due to the complexity of the involved measurement techniques, $CH_4$ isotope measurements have been limited mostly to relatively low frequency sampling in the field followed by isotope analysis in the laboratory (Bock et al., 2010; Brass and Röckmann, 2010; Sapart et al., 2011; Sperlich et al., 2013; Umezawa et al., 2009; Yamada et al., 2003). For many decades, the dominant method for high precision isotope analysis of atmospheric methane was isotope ratio mass spectrometry. In particular, the development of continuous-flow IRMS in the past two decades (Merritt et al., 1994; Merritt et al., 1995) has greatly increased the throughput of IRMS methods, making this the technique of choice in most laboratories, also because of the small sample amounts required.

Recently, mid-infrared laser absorption spectroscopy has proven its potential for high precision isotope ratio analysis. First attempts of measuring the isotopic composition of methane (Bergamaschi et al., 1998a; 1998b; 1994) were restricted to enhanced $CH_4$ fractions (>50 µmol/mol for $\delta^{13}C$ and >2000

Atmos. Chem. Phys. Discuss., doi:10.5194/acp-2016-60, 2016
Manuscript under review for journal Atmos. Chem. Phys.
Published: 10 February 2016


Atmospheric Chemistry and Physics Discussions

µmol/mol for δD) and required cryogenic cooling for both the laser source and the detector, which impeded in-situ and long-term applications. The invention of room temperature, quantum cascade laser (QCL) sources has triggered the development of a novel generation of spectrometers suitable for in-situ analysis of the isotopic composition of greenhouse gases (Eyer and al, 2015; Tuzson et al., 2008; Wächter et al., 2008). Their capability of high-temporal resolution led to new applications aiming for source attribution (Mohn et al., 2012; Tuzson et al., 2011; Wolf et al., 2015). The advantages of in-situ measurements are particularly apparent in combination with atmospheric modeling techniques, which enables the identification of specific source regions (Rigby et al., 2012; Sturm et al., 2013). Similarly, high-frequency, high-precision $CH_4$ isotope data are expected to greatly reduce uncertainties of national and global source estimations, as demonstrated in an observing system simulation experiment (Rigby et al., 2012).

In this paper we present the analytical setup and results of a 5-month campaign at the Cabauw tall tower site in the Netherlands, where the isotopic composition ($\delta^{13}C$ and δD) of $CH_4$ was measured with two instruments, one IRMS system developed at Utrecht University and one QCLAS-instrument developed at Empa. In the Methods section we describe the site, the experimental setup and the deployed isotope measurement techniques. In addition, descriptions of the modeling tools that were used to support interpretation of the dataset are given. In the Results section we present the dataset, including evaluation of the calibration and the compatibility of the techniques. In the Discussion section the results and new approaches for data evaluation of such high-resolution isotope datasets are discussed.

## 2. Methods

### 2.1. Site description

The 213 m tall tower is the central construction of the Cabauw Experimental Site for Atmospheric Research (CESAR, http://www.cesar-observatory.nl/, 51° 58' N, 4° 55' E, 2 m a.s.l.). The CESAR site is dedicated to atmospheric research and hosts a wide variety of instruments for in situ and remote sensing measurements of meteorological parameters, trace gases, pollutants, aerosols, and clouds. The

Atmos. Chem. Phys. Discuss., doi:10.5194/acp-2016-60, 2016
Manuscript under review for journal Atmos. Chem. Phys.
Published: 10 February 2016


Atmospheric Chemistry and Physics Discussions

site is located in an agricultural landscape, with $CH_4$ emissions originating from ruminants and other agricultural activities, but also from the peaty soil and the drainage ditches between the surrounding fields (Peltola et al., 2014). The small town Lopik (~7500 inhabitants) is located 1 km east of the tower. Population and road density increase steeply further away from the tower towards the country's major cities: Utrecht (at about 20 km distance), Rotterdam (30 km), the Hague (40 km) and Amsterdam (45 km). An estimated seven million people inhabit these cities and their many neighboring settlements. The location and surroundings are described in more detail in (Peltola et al., 2014; Peltola et al., 2015; Vermeulen et al., 2011). The instruments were operated in a room on the ground floor of the CESAR building. Since this room is not commonly used as laboratory, it has a limited air-conditioning capacity and the temperature varied between 25 ˚C and 30 ˚C.

### 2.2. Air sampling at the Cabauw tall tower

Air was continuously drawn through ½" o.d. Dekabon tubing from 20 m height at a total flow of 16 l $min^{-1}$ provided by a scroll pump (Varian Inc.). The sample gas flow was adjusted by means of a flow restriction at the inlet of the pump in order to maintain the pressure in the sampling line above 950 hPa. The sample gas flows for the methane isotope analyzers were branched off upstream of the scroll pump and the restriction, using ¼" o.d. Dekabon lines.

### 2.3. IRMS system

The new IRMS method for $\delta^{13}C$ and $\delta D$ analysis of atmospheric $CH_4$ is based on the ISAAC system as developed at the MPI for Biogeochemistry in Jena (W. Brand et al., manucript in preparation). Importantly, the system does not require liquid nitrogen coolant for the preconcentration and focusing steps, but uses a massive copper block cooled down to about -145 ˚C, to which the cold traps for preconcentration and cryo-focussing are connected via standoffs (see 2.3.1). This cold assembly is contained in an evacuated steel Dewar to prevent condensation of moisture. During the campaign, the extraction unit and two IRMS instruments (Thermo Delta Plus XL for hydrogen isotopes and Thermo Delta Plus XP for carbon isotopes) were operated at the CESAR site. The system is schematically

Atmos. Chem. Phys. Discuss., doi:10.5194/acp-2016-60, 2016
Manuscript under review for journal Atmos. Chem. Phys.
Published: 10 February 2016


Atmospheric Chemistry and Physics Discussions

shown in Fig. 1.

#### 2.3.1. Cryogenic trapping

A Polycold compact cooler compressor (Brooks Automation Inc., USA), filled with coolant PT-30, cooled a cold end on which a copper cylinder (70 mm diameter, 85 mm height, 3 kg) was mounted. In this configuration, the copper block reached a temperature of -145 ˚C. The pre-concentration trap (PreCon) was a 10 cm 1/8" SS tube filled with 4 cm 60/80 mesh HayeSep D in the center and 3 cm 60/80 glass beads on each end. It was connected with Valco fittings and the packing material was retained in the trap using removable frits (CEF1F). The focus trap (Focus) was a 10 cm 1/16" SS tube filled with 2 cm HayeSep D and 4 cm glass beads at both ends, connected with Valco fittings (ECEF211.0F). The traps could be heated with 0.5 m Thermsys heating wire wrapped around the tubes. The focus units were glued together with a PT-100 temperature sensor in heat-conducting two component epoxy on a brass standoff. These brass standoffs were mounted to the copper cylinder. In the "trapping" configuration the temperatures of the traps were usually kept at -135 ˚C.

#### 2.3.2. Measurement procedure

A 3-port 2-position Valco valve (3PV, Fig. 1) selected either ambient air drawn from the tower through a $Mg(ClO_4)_2$ dryer, or cylinder air that was injected via one port of an 8-port multiposition Valco valve (MPV). To check the system performance, a reference air cylinder (Ref) was measured alternately with ambient air, and three other target gas cylinders were measured occasionally. The inlet line was connected to a 4-port 2-position Valco valve (4PV1), which directed either Helium (He Air Products, BIP quality) or the selected airflow to the PreCon unit, which was connected in the loop position of a 6-port 2-position Valco valve (6PV). All He and air flows were controlled by MKS mass flow controllers (MFC).

The preconcentration and cryofocussing was done similarly to Brass and Röckmann (2010). After flushing the inlet line with >20 ml air, the 6PV was switched to the load position and air was admitted to the PreCon unit. The duration of the air sampling for the IRMS system was 10 minutes at a flow rate of

Atmos. Chem. Phys. Discuss., doi:10.5194/acp-2016-60, 2016
Manuscript under review for journal Atmos. Chem. Phys.
Published: 10 February 2016


Atmospheric Chemistry and Physics Discussions

5 ml $min^{-1}$ for $\delta^{13}C$ and 7 ml $min^{-1}$ for $\delta D$. The flow was provided by a Xavitech mini pump (P200-GAS-12V). During this step, the temperature measured at the PreCon stayed below -132 ˚C. At this temperature $CH_4$ and several other trace species were retained on the HayeSep D, while the air matrix was efficiently flushed out.

After preconcentration, the PreCon unit was heated to -30 ˚C and a He flow of 3 ml $min^{-1}$ transported the $CH_4$ in 90 seconds to the Focus unit, which was held at a temperature <-137 ˚C. After transfer of the sample to the Focus, the 6PV was switched to the load position and the PreCon was heated to -10 ˚C to release any remaining trapped gases such as $CO_2$.

The Focus was then heated to release the $CH_4$, which was directed via 4PV2 and 4VP3 either to the combustion oven and the Delta plus XP IRMS for $^{13}C$ analysis or to the pyrolysis oven and the Delta plus XL IRMS for D analysis.

For $\delta D$ analysis, the $CH_4$ was injected into a pyrolysis tube furnace (1400 ˚C), where $CH_4$ was converted to $H_2$ and carbon. The $H_2$ entered the IRMS, after passing a 2 m CarboPLOT column at room temperature (RT) and a nafion dryer, via the GasBench interface. No krypton interference (Schmitt et al., 2013) could be determined in this setup. The repeatability for $\delta D$ was generally better than ±2 ‰, based on consecutive analyses of reference air.

For $\delta^{13}C$, the $CH_4$ was injected from the cryofocus unit into a combustion oven containing a nickel / nickel oxide wire catalyst at 1100 ˚C, where the $CH_4$ was converted to $CO_2$ and $H_2O$. The resulting gas mixture passed a nafion dryer and a 10 m PoraPLOT Q column (5 ˚C) to eliminate interference from co-trapped krypton (Schmitt et al., 2013) before entering the IRMS via the GasBench interface. The repeatability of $\delta^{13}C$ was better than 0.07 ‰, based on consecutive analyses of reference air.

The typical measurement order during the Cabauw campaign was Ref $\delta^{13}C$ – Air $\delta^{13}C$ –Ref $\delta D$ – Air $\delta D$. A full measurement cycle took 84 min. On a regular base, pressurized air from a cylinder, applied as a target gas, was analyzed. The $CH_4$ mole fraction and isotopic composition in ambient air and target gas were calculated using an interpolation of the reference air analyzed before and afterwards. A custom made LabView software program was used to control and

Atmos. Chem. Phys. Discuss., doi:10.5194/acp-2016-60, 2016
Manuscript under review for journal Atmos. Chem. Phys.
Published: 10 February 2016


Atmospheric Chemistry and Physics Discussions

log the temperature of the traps, the valve switching and the flow setpoints of the MFCs.

#### 2.3.3. IRMS system isotope calibration

The isotope calibration of the IRMS system was based on a reference air cylinder that contains ambient air collected at the IMAU in 2014, with 1888 nmol/mol of $CH_4$ and isotope values of $\delta^{13}C$ = -47.75 ‰ and $\delta D$ = -88.6 ‰. The isotope calibration scale is based on the reference scale that was described in detail in Brass and Röckmann (2010). We used the average of the reference air measurement before and after the sample air measurement to calculate the mole fraction and δ values. The system linearity was monitored by injecting various amounts of reference air up to a $CH_4$ mole fraction equivalent to 2700 nmol/mol, and no non-linearity could be detected. Occasionally, the long-term stability of the system was checked by measuring 3 target cylinders with different $CH_4$ mole fractions and isotopic compositions. A robust link of the isotopic composition to the international reference materials VPDB and VSMOW has been established in the framework of the INGOS project (Sperlich et al., 2016).

### 2.4. QCLAS system

The analytical procedure of the laser based measurement system involves two steps: preconcentration of the $CH_4$ from 7.5 L of ambient air in a trace gas extractor (TREX) by adsorption on HayeSep D (Eyer et al., 2014; Mohn et al., 2010) and analysis of $CH_4$ isotopologues with a modified commercial QCLAS (QCL-76-D, Aerodyne Inc., USA). Details on the development, optimization and validation of the TREX-QCLAS system are given by Eyer et al. (2015).

The present manuscript comprises the first application of the TREX-QCLAS system for in-situ analysis of $CH_4$ isotopologues at a field site for an extended period of time. In comparison to the original setup, the heating power of the polyimide foil on the cold trap was reduced to 60 W to increase its lifetime. Due to the lower heating power the duration of the desorption step had to be extended, which led to an improved separation from residual bulk gases (e.g. $N_2$ and $O_2$) and thus a lower offset in $\delta^{13}C$ of 1.58 ‰ with respect to the MPI-scale, as compared to previously published results (Eyer et a., 2015). The offset was

Atmos. Chem. Phys. Discuss., doi:10.5194/acp-2016-60, 2016
Manuscript under review for journal Atmos. Chem. Phys.
Published: 10 February 2016


Atmospheric Chemistry and Physics Discussions

related to a higher $O_2$ mole fraction in the gas matrix after $CH_4$ preconcentration. One measurement cycle consisted of four consecutive measurements of ambient air samples and one sample of pressurized air used as a target gas, followed by a calibration phase and took around 4:30 hours.

A calibration gas (CG1, (1200 ± 50) µmol/mol $CH_4$, $\delta^{13}C$ = -(44.24 ± 0.10) ‰, $\delta D$ = -(104.7 ± 1.1) ‰) was diluted to 688 µmol/mol and analyzed between every preconcentrated sample as an anchor to correct the measurements for instrumental drift. A second calibration gas (CG2, (1103.8 ± 3.5) µmol/mol $CH_4$, $\delta^{13}C$ = -(36.13 ± 0.10) ‰, $\delta D$ = -(180.6 ± 1.1) ‰), diluted to a similar $CH_4$ mole fraction of 681 µmol/mol was used to calculate calibration factors for $\delta^{13}C$ and $\delta D$ values. Furthermore, gas cylinders of pressurized ambient air, referred to as target gas (TG1, TG2), were frequently measured over the entire campaign to determine and verify the repeatability of the measurement system, which was found to be 0.28 ‰ and 1.7 ‰ for $\delta^{13}C$ and $\delta D$ ($1\sigma$), respectively. Additional adjustments in the preconcentration procedure and in the analytical routine for isotope analysis improved the repeatability to 0.18 ‰ and 0.85 ‰ for $\delta^{13}C$ and $\delta D$ in the last month of the campaign.

The $CH_4$ isotopic composition of the calibration gases, as well as the target gases (TG1, (2639.5 ± 0.6) nmol/mol $CH_4$, $\delta^{13}C$ = -(46.48 ± 0.10) ‰, $\delta D$ = -(119.0 ± 1.1) ‰, TG2, (2659.8 ± 0.6) nmol/mol $CH_4$, $\delta^{13}C$ = -(45.87 ± 0.10) ‰, $\delta D$ = -(114.1 ± 1.1) ‰) were determined by the Stable Isotope Laboratory at the Max-Planck-Institute for Biogeochemistry. $CH_4$ mole fraction measurements were linked to the WMO-X2004 calibration scale (Dlugokencky et al., 2005) through calibration of the target gases against NOAA reference standards at Empa.

### 2.5. Modeling

Two complementary atmospheric transport models (TM5, FLEXPART-COSMO), both in combination with two different emissions inventories (TNO-MACC_2, EDGAR/LPJ-WhyMe), were applied to support interpretation of the measurements. The Eularian tracer model TM5 simulated the distribution of $CH_4$ and $^{13}CH_4$ at global scale with a zoom on Europe at 1° x 1° resolution and considered both the isotopic signatures of different sources and the fractionation

Atmos. Chem. Phys. Discuss., doi:10.5194/acp-2016-60, 2016
Manuscript under review for journal Atmos. Chem. Phys.
Published: 10 February 2016




by different removal pathways of $CH_4$ in the atmosphere. The Lagrangian particle dispersion model FLEXPART-COSMO, conversely, was run in backward mode at a higher resolution of 0.06° x 0.06° but only over Europe. This model is better able to represent the spatial variability of $CH_4$ sources in the near field of Cabauw but it only simulated the contributions from the last 4 days of emissions within Europe and not the large-scale background. Chemical loss of $CH_4$ was not considered due to the short transport times between the sources and the receptor point at Cabauw. δD was only simulated with FLEXPART-COSMO.

#### 2.5.1. TM5 modeling

Simulations of atmospheric $CH_4$ and $\delta^{13}C$ were performed using the global tracer model TM5 (Krol et al., 2005). The Eularian off-line model was driven by meteorological fields from the European Centre for Medium Range Weather Forecast (ECMWF) reanalysis project Era-Interim (Dee et al., 2011), pre-processed for use in TM5. For vertical transport due to moist convection we made use of Era Interim archived convective mass fluxes, replacing the use of the Tiedke scheme in Krol et al. (2005). The model was run at a horizontal resolution of $6^o x 4^o$ globally and $1^o x 1^o$ inside a zoom domain covering Western Europe. The model uses 25 hybrid sigma-pressure levels from the surface to top of atmosphere.

Two parallel (forward) TM5 simulations were performed with $CH_4$ and $^{13}CH_4$ as transported tracers. In the standard configuration, anthropogenic $CH_4$ emissions were taken from EDGAR4.2 FT2010 (EDGAR, 2009), extrapolated to 2014 and 2015 using annual statistics from the Food and Agriculture Organization of the United Nations (FAO) and the British Petroleum Company (BP), as described in Houweling et al. (2014). For natural wetland emissions, an average of the emission estimates derived by Spahni et al. (2011) for the period 2003-2008 was taken, using the LPJ-WhyMe model. For a complete description of the $CH_4$ emissions (Table 1), see Monteil et al. (2013) and references therein. $^{13}CH_4$ emissions were derived from the $CH_4$ emissions using prescribed $\delta^{13}C$ source signatures (see Table 1). The source signature confidence intervals were taken from existing literature. The actual source signatures were adjusted within these ranges to bring the background $\delta^{13}C$ level to good agreement with observations

Atmos. Chem. Phys. Discuss., doi:10.5194/acp-2016-60, 2016
Manuscript under review for journal Atmos. Chem. Phys.
Published: 10 February 2016




(Monteil et al., 2011). In a second set of simulations, anthropogenic emissions in a regional domain centered on Cabauw were replaced by emissions from the European TNO-MACC_2 inventory, which was used as the standard inventory in the FLEXPART-COSMO simulations (see below). Outside the regional domain covered by TNO-MACC_2, the EDGAR emissions were used.

Atmospheric removal of $CH_4$ was modeled as described in Monteil et al. (2013), using kinetic fractionation factors $\alpha = k(^{12}C) / k(^{13}C)$ of $\alpha_{OH} = 1.0055$, $\alpha_{Cl} = 1.066$ and $\alpha_{O(1D)} = 1.013$ for the reactions between $CH_4$ and OH (Sander et al., 2006), Cl (Saueressig et al., 1995) and $O(^1D)$ (Saueressig et al., 2000), respectively. Simulations of the period 2005-2015 were used to calculate a realistic state of the atmosphere at the start of the measurement campaigns. Time series were extracted from model-simulated mole fraction fields after interpolation to the horizontal coordinate and height of the Cabauw tower air inlet.

### 2.5.2. FLEXPART-COSMO modeling

The Lagrangian Particle Dispersion Model (LPDM) FLEXPART (Stohl et al., 2005) was used in a modified version coupled to the mesoscale numerical weather forecast model COSMO (Baldauf et al., 2011) to simulate the regional contribution of different source categories to the concentrations and isotopic signatures of $CH_4$ at Cabauw. FLEXPART–COSMO was driven by hourly operational analysis fields generated by the Swiss national weather service MeteoSwiss for a domain covering entire western and central Europe from Ireland, Denmark, Poland in the north to Portugal and southern Italy in the south with a horizontal resolution of approximately 7 km x 7 km and 60 vertical levels. Every 3 hours, 50'000 particles (air parcels) were released from the position of the inlet 20 m above surface and traced backward in time for 4 days to compute the sensitivity of each 3-hourly measurement to upwind sources. The corresponding source sensitivity maps or footprints (Seibert and Frank, 2004) were multiplied with gridded $CH_4$ emissions to compute the mole fraction enhancement above background expected from different sources. Emissions were taken from the TNO-MACC_2 inventory for Europe representative of the year 2009 and available at 0.125° x 0.0625° resolution (Kuenen et al., 2014) or,

Atmos. Chem. Phys. Discuss., doi:10.5194/acp-2016-60, 2016
Manuscript under review for journal Atmos. Chem. Phys.
Published: 10 February 2016


Atmospheric Chemistry and Physics Discussions

368 alternatively, from the same version of EDGAR/LPJ-WhyMe inventory driving
369 TM5 at a resolution of 1° x 1°. This was done separately for a number of SNAP
370 (Standardized Nomenclature for Air Pollutants) source categories with specific
371 isotopic signatures as summarized in Table 2.

372 For the domain covered by the FLEXPART-COSMO simulations, which includes
373 most of western and central Europe, total anthropogenic emissions are 20.6 Tg
374 $CH_4$/yr in EDGAR and 18.3 Tg $CH_4$/yr in TNO-MACC, which corresponds to a
375 difference of 12.5%. $CH_4$ emissions from gas/oil production and distribution are
376 89% higher, $CH_4$ emissions from agriculture 19% lower and $CH_4$ emissions from
377 waste 12% higher in EDGAR than in TNO-MACC.

378 Source specific emissions were combined with isotopic signatures of the various
379 categories from Table 2 to derive $\delta^{13}C$ and $\delta D$ isotope source signatures for the
380 $CH_4$ that was picked up by the air parcel along the trajectory.

381 **2.6. Interpretation of $CH_4$ isotope data**

382 **2.6.1. Data analysis by a Keeling plot technique**

383 The isotopic source signatures of $CH_4$ emissions were estimated using the
384 Keeling plot technique (Keeling, 1961; Pataki et al., 2003). This method allows
385 determining the isotopic composition of a source that mixes into a background
386 reservoir from the observed ambient isotopic composition and mole fraction. An
387 implicit assumption of the Keeling plot approach is that the isotopic composition
388 and mole fraction of the background reservoir and the isotopic composition of
389 the source stay constant over the time range of the analysis. This may not always
390 apply as $CH_4$ may originate from different sources and their relative contribution
391 may change over time.

392 To exploit the high temporal resolution of our data, we applied a novel approach
393 of a moving Keeling plot (MKP) method. Data within a moving window of 12
394 hours were used to calculate the source isotopic composition. This window was
395 moved in 1-hour time steps over the data series. In addition, values for
396 background conditions within a 48-hour period, centered on the respective 12-
397 hour window, were included in the analysis. These background values were
398 chosen between 10:00 and 18:00 local time, because during this period a

Atmos. Chem. Phys. Discuss., doi:10.5194/acp-2016-60, 2016
Manuscript under review for journal Atmos. Chem. Phys.
Published: 10 February 2016


Atmospheric Chemistry and Physics Discussions

convective boundary layer usually develops and hence local influence is weak; pollution events with $CH_4$ mole fractions above 2100 nmol/mol were filtered out additionally. For each time window, an orthogonal least squares fit was applied to the δ values vs. the inverse $CH_4$ mole fractions and $R^2$ values were calculated. A Keeling plot analysis only returns meaningful values for the source isotopic composition if the variations in $CH_4$ mole fraction are significant and if the emissions are from a source with a well-defined isotopic composition. Therefore, two additional filters were applied: i) the mole fraction had to vary by more than 200 nmol/mol within each time window and ii) the $R^2$ of the fit had to be larger than 0.8. If $R^2 < 0.8$, the 12 h interval was reduced consecutively by one hour to a minimum of six hours until either the $R^2$ of the fit was > 0.8 or the number of data points was lower than five. On average this technique accumulated 22 data points per 12-h time window.

## 3. Results

### 3.1. Overview of the field measurements at the Cabauw site

The full record of the methane mole fraction and isotopic composition obtained with the two measurement techniques at the CESAR site is shown in Fig. 2. The IRMS system started with δD measurements first, and after 3 weeks delivered both $\delta^{13}C$ and δD data. The TREX-QCLAS system started later and ran continuously from mid-December to mid-January, and from mid-February to the end of the campaign. Despite a number of interruptions mainly due to various kinds of instrument malfunction, the combined time series of both techniques shows a high temporal coverage with more than 2500 measurements performed for both $\delta^{13}C$ and δD.

A qualitative inspection of the time series already conveys the obvious features that will be discussed below in more detail: the methane mole fraction $\chi(CH_4)$ shows a large number of substantial increases above background level, and these positive methane excursions are accompanied by negative excursions in the δ values from the background level. Thus the additional methane is generally depleted in both $^{13}C$ and D.

### 3.2. Intercalibration of the two analytical techniques

Atmos. Chem. Phys. Discuss., doi:10.5194/acp-2016-60, 2016
Manuscript under review for journal Atmos. Chem. Phys.
Published: 10 February 2016


Atmospheric Chemistry and Physics Discussions

Before presenting a detailed analysis of the $CH_4$ isotopic composition in ambient air, we compare the results obtained with the IRMS and QCLAS techniques in order to evaluate their performance and to combine the results into one final dataset. Although both systems measured air from the same intake line, the sampling intervals could not be synchronized since both instruments operated in different measurement cycles. A full measurement cycle (including measurement of the reference gas) took 84 minutes for the IRMS system and 54 minutes for the TREX-QCLAS system. The actual duration of the air sampling was 10 minutes for the IRMS system and 15 minutes for the QCLAS system. So even if the systems coincidentally started sampling at the same time, they never actually analyzed exactly the same air mass. Consequently, differences between the systems contain contributions from natural variability, random fluctuations due to limited measurement precision, and system offsets. Fig. 3 shows a comparison of the $\chi(CH_4)$, as well as $\delta^{13}C$ and $\delta D$ values that were obtained with the TREX-QCLAS and the IRMS technique. To visualize the possible effect of time shifts, the size of the points corresponds to the proximity of the sampling intervals. A total of 727, 333 and 277 measurement pairs for $\chi(CH_4)$, $\delta^{13}C$ and $\delta D$, respectively, analyzed by both techniques were combined in this way.

The mole fraction comparison shows good agreement along the 1:1 line but with a large scatter, which has two contributions: i) instrumental noise, as the isotope systems have a relatively large uncertainty for measurement of the mole fraction compared to existing high-precision $CH_4$ analyzers, and ii) natural variability associated with the sampling of different air masses as described above. The second point is supported by the fact that the average difference in $CH_4$ mole fractions between the two analytical techniques was larger for larger temporal differences in the sampling intervals.

For the isotope intercalibration plots, the grey-black shading of the circles indicates the difference in $\chi(CH_4)$ of the respective measurement pair analyzed by both techniques. The overall difference between the measurements conducted with the two systems (QCLAS-IRMS) is +(0.05± 0.03) ‰ for $\delta^{13}C$ and −(3.6 ± 0.4) ‰ for $\delta D$ (the stated errors are standard errors of the mean). The mean offsets of 0.05 ‰ for $\delta^{13}C$ and 3.6 ‰ for $\delta D$ are well within the WMO

Atmos. Chem. Phys. Discuss., doi:10.5194/acp-2016-60, 2016
Manuscript under review for journal Atmos. Chem. Phys.
Published: 10 February 2016




462 extended compatibility goals of 0.2 ‰ for $\delta^{13}C$ and 5 ‰ for δD, as indicated by
463 the red dashed lines (WMO, 2014). Individual measurement pairs, however, can
464 show significantly larger deviations for aforementioned reasons. The mean offset
465 values determined above were applied to the QCLAS data to create one combined
466 dataset with 2610 data points for $\delta^{13}C$ and 2673 data points for δD.

467 **3.3. FLEXPART-COSMO source attribution**

468 In FLEXPART-COSMO, the contributions of the individual source types are
469 simulated separately and added up to obtain the cumulative $CH_4$ mole fraction.
470 Figure 4 shows these contributions in absolute (top) and relative terms
471 (bottom). According to the model, the relative contributions at the Cabauw site
472 are quite uniform, with agricultural sources accounting for more than 60%,
473 waste (mostly landfills) around 20–40%, and fossil sources between 0 and 40%.
474 We note that significant contributions from fossil sources are only detected
475 episodically, during several events that usually last a few days. Contributions
476 from other source categories are generally negligible at the Cabauw site.

477 **3.4. TM5 and FLEXPART-COSMO modeling including isotopes**

478 The TM5 model calculates the combined influence of the global methane sources
479 and sinks on $CH_4$ and $\delta^{13}C$ at the Cabauw tower, and therefore the TM5 results
480 can be compared directly to the measured time series. For FLEXPART-COSMO, a
481 representative background mole fraction and isotopic signature needs to be
482 added for comparison with the observations. For simplicity we assumed a
483 constant background similar to the observed values for background conditions:
484 1930 nmol/mol for $\chi(CH_4)$ with $\delta^{13}C$ = -47.1 ‰ and δD = -86 ‰.

485 Figure 5 shows a comparison of these model-generated time series with the
486 measured data for the entire campaign. Both models capture the amplitude and
487 the temporal variability of $\chi(CH_4)$well. Most of the methane pollution events
488 observed at the CESAR site are also present in the modeled time series and the
489 increase in $\chi(CH_4)$ is of a comparable size. In addition, the results of the TM5 and
490 the FLEXPART-COSMO model for $CH_4$ mole fractions agree relatively well with
491 each other ($R^2$=0.69), in particular when both models are run with the same
492 inventory at the same coarse spatial resolution, i.e. with EDGAR/LPJ-WhyMe.

Atmos. Chem. Phys. Discuss., doi:10.5194/acp-2016-60, 2016
Manuscript under review for journal Atmos. Chem. Phys.
Published: 10 February 2016


Atmospheric Chemistry and Physics Discussions

493 A few pronounced $CH_4$ events in Figure 5 show larger differences between the
494 models. On 2 November, FLEXPART-COSMO simulates an emission signal that is
495 not captured by TM5. Unfortunately no measurements are available for this
496 event to decide on which model performs better. On 30 November TM5
497 simulates a $CH_4$ plume, which is absent in FLEXPART-COSMO, and this event is
498 also not supported by the measurements. Nevertheless, the overall performance
499 of the TM5 global model is remarkable given its coarse spatial resolution. The
500 global model has the advantage that it includes the influence of long-range
501 transport. As expected, however, the observed variability is predominantly
502 influenced by local and regional emissions.

503 Regarding the time series of the δ values, both TM5 and FLEXPART-COSMO
504 qualitatively display the expected anti-correlations between $CH_4$ and $\delta^{13}C$.
505 However, the amplitude of the $\delta^{13}C$ variability is generally underestimated in the
506 model runs, especially when using the EDGAR inventory. In addition, the
507 modeled background level of $\delta^{13}C$ in TM5 is offset by up to 1 ‰, but this is
508 consistent with data-model comparisons at clean background sites at mid
509 latitudes (not shown).

510 Using the TNO-MACC inventory in FLEXPART-COSMO results in better
511 agreement with the observed variability of $\delta^{13}C$. In TM5, the TNO-MACC
512 emissions reduce the amplitude of the $CH_4$ variability, which is explained by the
513 13% lower emissions in TNO-MACC compared with EDGAR. Furthermore, the
514 results of both models are consistent with the emissions being more depleted in
515 $\delta^{13}C$ in TNO-MACC than in EDGAR. The measurements indicate emissions that
516 are even more depleted in $\delta^{13}C$ than TNO-MACC values. These results suggest
517 that the fractional contribution of isotopically heavy fossil emissions is
518 overestimated in EDGAR, at least in the area sampled by Cabauw, although the
519 uncertainty in the assumed $\delta^{13}C$ source signatures could also contribute. For
520 instance, recent literature showed, that landfill emissions from the UK are more
521 depleted in $^{13}CH_4$ due to the implementation of gas extraction systems (Zazzeri
522 et al., 2015).

523 The δD time series simulated with FLEXPART-COSMO using the TNO-MACC
524 inventory is in good agreement with the measurements. This further indicates

Atmos. Chem. Phys. Discuss., doi:10.5194/acp-2016-60, 2016
Manuscript under review for journal Atmos. Chem. Phys.
Published: 10 February 2016




that TNO-MACC has a realistic source mixture, but the uncertainties in the δD source signatures are too large to draw firm conclusions at this stage. Despite these uncertainties, Figure 5 clearly demonstrates how isotopic measurements highlight differences between emission inventories, which would go unnoticed looking only at $CH_4$ mole fractions. Additional information may be available from the combination of both isotope signatures. For several of the $CH_4$ elevation events shown in Fig. 5b, the relative changes in $\delta^{13}C$ and δD modeled with FLEXPART-COSMO vary when using the two different inventories (TNO-MACC and EDGAR). Some of the anomalies show differences pointing in the same direction for $\delta^{13}C$ and δD, and some others not. This suggests that δD provides additional independent information, which will be discussed in more detail in Section 4.3 using a double isotope plot of the source signatures (Fig. 7). The benefit of the high-resolution dual isotope measurements for validating emissions used in the models will be investigated in Section 4.4.

# 4. Discussion

## 4.1. Diurnal and synoptic variability

A prominent feature of the high-resolution dataset is the pronounced diurnal variability, with large increases in $CH_4$ mole fraction that occur often during the night, due to the shallow planetary boundary layer. In addition, there are also several synoptic (but much smaller) pollution events, where $CH_4$ mole fractions stay above the unpolluted background level for several days. These elevations are likely caused by synoptic scale advection of $CH_4$ plumes from other source regions with a different source mix.

## 4.2. Isotope identification of the cumulative source

In Fig. 6, the Keeling plot technique is applied to identify the isotopic signature ($\delta^{13}C$, δD) of the combined $CH_4$ emissions detected at the Cabauw site. An orthogonal regression method was applied to determine the fit parameters. This analysis yields well-defined isotopic signatures of the cumulative source (the y-intercept of the regression analysis) of $\delta^{13}C$ = -(60.9 ± 0.2) ‰ and δD = -(295 ± 1) ‰. The inferred isotopic signature agrees well with emission from ruminants, which are expected to be the main source of $CH_4$ in this rural area. This is

Atmos. Chem. Phys. Discuss., doi:10.5194/acp-2016-60, 2016
Manuscript under review for journal Atmos. Chem. Phys.
Published: 10 February 2016




plausible, because the cumulative source signature is largely determined by the pronounced nighttime $CH_4$ elevations, which represent the local emissions close to the tower. Also the source contributions modeled by FLEXPART-COSMO suggest the dominant influence of agricultural emissions in this rural area (Fig. 4). Interestingly, the source signature for the much smaller synoptic $CH_4$ variations of the background (red points in Fig. 6) is not significantly different from the one for the complete dataset.

### 4.3. Short-term variability

Given the high temporal resolution of the dataset presented here, the isotope variations can be interpreted in much more detail than the overall analysis performed above. This allows identifying varying contributions of $CH_4$ sources during different periods of the campaign. To do so, we applied a 12-hour Moving Keeling Plot (MKP) method to the data, as described in Sect 2.6.1.

Fig. 7 summarizes the results of the MKP method in the form of a $\delta D$ vs. $\delta^{13}C$ plot. To combine $\delta^{13}C$ and $\delta D$ measurements performed at different times, MKP intercepts were averaged over 6 h intervals. $\delta^{13}C$ source signatures range between -68 ‰ and -55 ‰ and $\delta D$ source signatures cover a relatively wide range between -350 ‰ and -230 ‰, indicating emissions mainly from microbial sources as derived from the cumulative Keeling plot analysis. During some periods, however, elevated $\delta^{13}C$ and $\delta D$ source signatures reveal significant additional contributions from waste and/or fossil emissions.

The colored symbols in Fig. 7 highlight the source signatures of three 48 h events (10-12, 16-18 and 22-24 March) that are discussed in more detail in the following. For the event of 16-18 March, selected results of the 12 h MKP method are displayed in Fig. 8**,** demonstrating the advantage of the high temporal resolution data. It is possible to clearly distinguish variations in the isotopic source signatures during this event by variations in the y-axis intercepts. The increase by about 6 ‰ for $\delta^{13}C$ and about 50 ‰ for $\delta D$, in the source isotopic signature for this event, clearly indicates the gradually increasing contribution of $CH_4$ from isotopically enriched sources, e.g. fossil fuel- or waste-related $CH_4$.

Atmos. Chem. Phys. Discuss., doi:10.5194/acp-2016-60, 2016
Manuscript under review for journal Atmos. Chem. Phys.
Published: 10 February 2016




The temporal evolution of the observed source mixture is investigated in further detail in Fig. 9, where the 16-18 March period (labeled as 2) is compared to two other 48 h – periods (10-12 March; label 1, and 22-24 March; label 3), each with significant diurnal $CH_4$ elevations. For event 1, the isotope source signatures stayed rather constant at values around $\delta^{13}C$ = -62 ‰ and $\delta D$ = -320 ‰. These values are typical for microbial emissions from an agricultural source and agree well with the source contributions predicted for this period by the FLEXPART-COSMO model.

Period 2 is characterized by much stronger isotopic change within the 48 h period. The $\delta^{13}C$ source signature increases to above -60 ‰ and the $\delta D$ source signature increases to -240 ‰ by the end of the period (see Fig. 9). The double-isotope plot in Fig. 7 shows that the change in $\delta D$ during event 2b clearly points towards fossil fuel sources, which provides independent support for the FLEXPART-COSMO simulations, where the contributions from fossil-fuel-derived emissions are higher for the second day.

For period 3, the $\delta^{13}C$ source signatures increased during the 48 h by about 2-3 ‰, whereas the $\delta D$ signatures remained constant around -300 ‰. For this period, the double isotope plot of Fig. 7 indeed shows a shift towards the waste category. Also this observation is independently confirmed (at least qualitatively) by the FLEXPART-COSMO model derived source attribution, which indicates the largest fraction of waste-derived $CH_4$ for the first day and a small addition of fossil $CH_4$ for the second day of event 3. These examples show that even at a location like Cabauw, where one source category strongly dominates, contributions from isotopically different sources can be identified if sufficiently high-resolution dual isotope ratio data are available. We note that the "directional" information in the double isotope plot is only available by combining $\delta^{13}C$ and $\delta D$ measurements. It would be much harder, if not impossible, to detect an addition from fossil fuel- or landfill- derived $CH_4$ based on $\delta^{13}C$ or $\delta D$ data alone.

### 4.4. Evaluation of emission databases with high temporal resolution $CH_4$ isotope data

Atmos. Chem. Phys. Discuss., doi:10.5194/acp-2016-60, 2016
Manuscript under review for journal Atmos. Chem. Phys.
Published: 10 February 2016


Atmospheric Chemistry and Physics Discussions

As described in Section 3.4, both the TM5 and the FLEXPART-COSMO model-generated time series of $CH_4$ mole fractions show an adequate agreement with the $CH_4$ measurements at the Cabauw site. Therefore, the comparison between measurement data and the models can be used to evaluate the methane budget in more detail. In this context, the measured and modeled isotopic source signatures can be employed to assess the validity of emission inventories, EDGAR and TNO-MACC, with respect to the magnitude and spatial distribution of source categories. To compare the measured isotopic source signatures to the model results, the simulated isotope time series were linearly interpolated and evaluated in the same way as the observations using the 12 h MKP method. This analysis was performed for both models (TM5 and FLEXPART-COSMO), each using both the EDGAR/LPJ-Why-Me and the TNO_MACC inventories. Additionally, isotopic source signature time series were calculated directly from FLEXPART-COSMO data, without using of the MKP method. This direct method allowed an independent estimation of the source signatures and, thus, also provided an opportunity to evaluate the MKP method.

The statistics of the isotope source signatures from all four model-inventory combinations are shown as histograms in Fig. 10, together with the measurement-derived source signatures and the directly derived source signatures from FLEXPART-COSMO modeling. A clear difference can be observed between the source signatures derived with the two different emission inventories. Model runs with the EDGAR/LPJ-WhyMe emission inventory (red in Fig. 10) tend to produce $CH_4$ isotope source signature distributions that are more enriched in $^{13}C$ and D than the model runs with TNO-MACC emissions. These differences are very similar for the simulations using TM5 and FLEXPART-COSMO, suggesting that differences originate from the emission inventories, rather than from differences between the models themselves. The $\delta^{13}C$ source signatures derived from the measurements at the Cabauw tower are even significantly more depleted than any of the model-generated datasets. For $\delta D$, the source signatures using TNO-MACC emissions are relatively close to the measurements at Cabauw, whereas the values using EDGAR emissions are much more enriched in $CH_3D$.

Atmos. Chem. Phys. Discuss., doi:10.5194/acp-2016-60, 2016
Manuscript under review for journal Atmos. Chem. Phys.
Published: 10 February 2016




649 The high temporal resolution isotope data that are described in this paper thus
650 provide relevant information to further constrain models and/or emission
651 inventories, because the isotope source signatures can change rapidly. The
652 comparison of our first high-resolution isotope measurements at Cabauw to
653 model calculations clearly identify differences between the modeled inventories,
654 where the EDGAR inventory produced too enriched source signatures due to a
655 higher contribution from fossil fuel sources. Similar differences in terms of
656 source contributions between EDGAR and TNO-MACC_2 were also reported by
657 Hiller et al. (2014) for Switzerland, and Henne et al. (2015) concluded that
658 natural gas emissions in Switzerland are likely overestimated in EDGAR.

659 **5. Conclusions and outlook**

660 The dual isotopic composition of $CH_4$ has been monitored for the first time with
661 high temporal resolution in an extended (5 months) field deployment with two
662 different instruments, an IRMS system and a QCLAS system, at the tall tower site
663 Cabauw, the Netherlands. The measurements of both instruments compare well
664 and can be combined to a time series of more than 2500 measurements for both
665 $\delta^{13}C$ and $\delta D$. Using a moving Keeling plot technique, the isotopic source
666 signatures of periods with significant $CH_4$ elevations can be derived with high
667 temporal resolution. The combination of $\delta^{13}C$ and $\delta D$ data provides strong
668 constraints to distinguish emissions from different source categories. Overall,
669 $CH_4$ emissions at the Cabauw tall tower are dominated by agricultural sources,
670 but variations in the source signatures allow identification of events with
671 increased contributions from fossil fuel and waste sources, which can be used to
672 validate variations in the source mix, calculated using the FLEXPART-COSMO
673 model.

674 The high-resolution isotope ratio measurements at Cabauw were compared to
675 model calculations that used two different emission inventories. When two very
676 different models (TM5 and FLEXPART-COSMO) used emissions from the EDGAR
677 inventory, they produced clearly too enriched source signatures. The modeled
678 source signatures were systematically more depleted and closer to the measured
679 ones when the TNO-MACC inventory was used. The differences in the source
680 signatures appear to originate from differences in the inventories and not from



differences in the models, which supports indications in the recent literature that fossil fuel related emissions might be overestimated in EDGAR. We note that measurements at Cabauw reflect only one limited region of the European domain, and given the many degrees of freedom (transport, source signatures used in the models, emission inventories), one single dataset is not sufficient to make a final decision on the quality of the emission dataset. High frequency analysis of $\delta^{13}C$- and $\delta D$ at several locations would allow better constraints on isotope source signatures and emissions in atmospheric models. Our proof-of-concept study presented here using continuous high-resolution techniques shows that this will be feasible in the future.

## Acknowledgements

This project was funded by the European Community's Seventh Framework Program (FP7/2007-2013) within the InGOS project under grant agreement No. 284274. Additional funding from the Swiss National Science Foundation (SNSF) within grant No. 200021_134611 and TNA grants within INGOS is gratefully acknowledged. The campaign at the Cabauw tall tower was made possible with strong support from Marcel Brinkenberg (KNMI), Michel Bolder and Henk Snellen (IMAU). We also thank Marco Weber (Empa) for assistance during transport and setup of the TREX-QCLAS system at the CESAR site.

## Author contributions

S.E. and C.vdV. carried out the isotope measurements at the Cabauw tower. C.vdV., T.R. and W.A.B. developed the IRMS system. S.E., B.T., L.E. and J.M. developed the TREX-QCLAS system. C.vdV., S.E., J.M., T.R., B.T., M.E.P., G.Z., D.L., E.G.N., and J.M.N. contributed to the Cabauw measurement campaign. G.M., S.H. and D.B. performed the modeling with TM5 and FLEXPART-COSMO. S.E., T.R., J.M., B.T., E.H., D.B., G.M., S.H., C.vdV., M.E.P. and H.F. performed and contributed to the data evaluation. S.E. produced the figures for the manuscript. T.R., S.E. and J.M. wrote the manuscript with input from C.vdV., G.M., S.H., E.H., D.B., H.F. and L.E. T.R., L.E. and J.M. designed the study as part of the INGOS project.

Atmos. Chem. Phys. Discuss., doi:10.5194/acp-2016-60, 2016
Manuscript under review for journal Atmos. Chem. Phys.
Published: 10 February 2016


Atmospheric Chemistry and Physics Discussions

711 **Table 1** European $CH_4$ emissions and isotope source signatures ($\delta^{13}C$, $\delta D$) for the
712 different source categories used in TM5.

| Process | Yearly emissions (Europe, Tg $CH_4$/yr) | source signature $\delta^{13}C$/‰ |
|---|---|---|
| **Natural emissions** | **22.1** | **-59.2** |
| Natural wetlands (1) | | |
| *Peatland* | 9.3 | -68 |
| *Wet mineral soils* | 4.6 | -65 |
| *Inundated wetlands* | 1.3 | -60 |
| Geological emissions (2) | 6.5 | -42 |
| Termites (3) | 0.4 | -63 |
| **Anthropogenic emissions** | **45.3** | **-52.4** |
| Biomass burning (4) | 0,3 | -23.6 |
| Agriculture (5) | | |
| *Domestic ruminants* | 11 | -64 |
| *Manure* | 3 | -54 |
| *Rice paddies* | 0.17 | -65 |
| Energy sector (5) | | |
| *Coal mining* | 3.4 | -47 |
| *Oil production* | 3 | -42 |
| *Gas production and distribution* | 12 | -42 |
| *Oil combustion* | 0.41 | -32 |
| Residential sector (5) | 1.6 | -32 |
| Waste treatment (5) | | |
| *Landfills* | 9 | -54 |
| *Waste waters* | 3 | -50 |
| **Total** | **67.4** | **-54.6** |

713 (1) Spahni et al. (2011); (2) Etiope et al. (2008); (3) Sanderson et al. (1996); (4)
714 GFED3/4 (http://www.globalfiredata.org/); (5) EDGAR4.2FT (EDGAR, 2010).
715

Atmos. Chem. Phys. Discuss., doi:10.5194/acp-2016-60, 2016
Manuscript under review for journal Atmos. Chem. Phys.
Published: 10 February 2016


Atmospheric Chemistry and Physics Discussions

716 **Table 2** SNAP (Standardized Nomenclature for Air Pollutants) source categories
717 and corresponding $\delta^{13}C$ and $\delta D$ source signatures from the TNO-MACC_2
718 inventory as used in FLEXPART-COSMO.

| SNAP Category | Description | $\delta^{13}C$/‰ | $\delta D$/‰ |
|---|---|---|---|
| 1 | Energy industries, oil or gas production | -42 | -175 |
| 2 | Residential combustion | -32 | -175 |
| 3+4 | Industrial combustion and non-combustion processes | -60 | -175 |
| 5 | Extraction and distribution of fossil fuels including distribution of natural gas | -42 | -175 |
| 7 | Road transport | -20 | -175 |
| 9 | Waste including emissions from landfills | -54 | -293 |
| 10 | Agriculture including emissions from ruminants and manure management | -64 | -319 |
| 6+8 | Other emissions (negligible) | -42 | -175 |

719

Atmos. Chem. Phys. Discuss., doi:10.5194/acp-2016-60, 2016
Manuscript under review for journal Atmos. Chem. Phys.
Published: 10 February 2016


Atmospheric Chemistry and Physics Discussions

720 Table 3. Mean value and standard deviation of the histograms of the source
721 isotopic composition shown in Figure 10.

| **Model + Inventory** | **Method** | **$\delta^{13}C$/‰** | **$\delta D$/‰** |
|---|---|---|---|
| Measurement data | MKP | -60.9 ± 3.1 | -301 ± 24 |
| TM5 + Edgar | MKP | -53.3 ± 1.1 | |
| FLEXPART-COSMO + Edgar | MKP | -54.5 ± 1.6 | -277 ± 10 |
| FLEXPART-COSMO + Edgar | Direct | -53.4 ± 1.7 | -269 ± 10 |
| TM5 + TNO-MACC | MKP | -56.7 ± 0.8 | |
| FLEXPART-COSMO + TNO-MACC | MKP | -57.6 ± 1.9 | -294 ± 12 |
| FLEXPART-COSMO + TNO-MACC | Direct | -57.2 ± 1.7 | -289 ± 11 |

722

Atmos. Chem. Phys. Discuss., doi:10.5194/acp-2016-60, 2016
Manuscript under review for journal Atmos. Chem. Phys.
Published: 10 February 2016


Atmospheric Chemistry and Physics Discussions

723 **Figures**

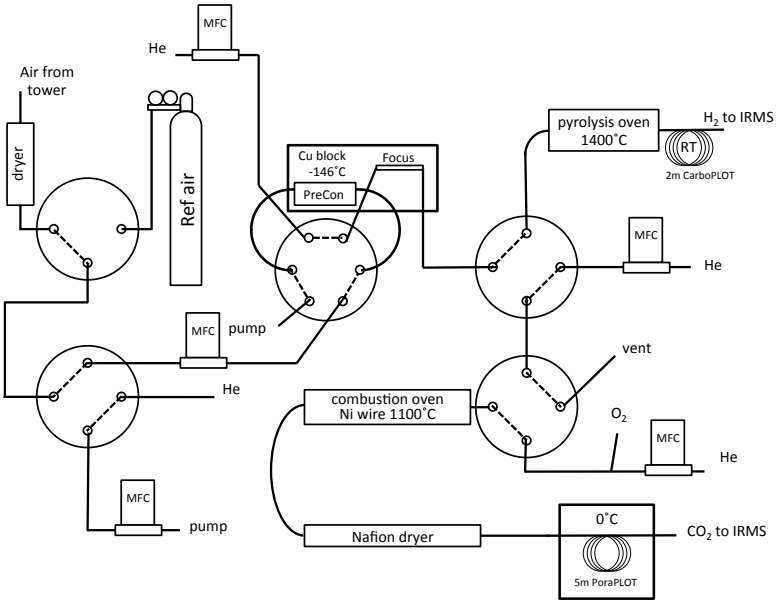


724 Fig. 1: Schematics of the pre-concentration and extraction system developed for
725 the IRMS technique. MFC denotes mass flow controller. The 8-port valve through
726 which the Ref air bottle was connected to the first selection valve is not shown to
727 reduce complexity. For further description see the main text.

728

729

Atmos. Chem. Phys. Discuss., doi:10.5194/acp-2016-60, 2016
Manuscript under review for journal Atmos. Chem. Phys.
Published: 10 February 2016


Atmospheric Chemistry and Physics Discussions

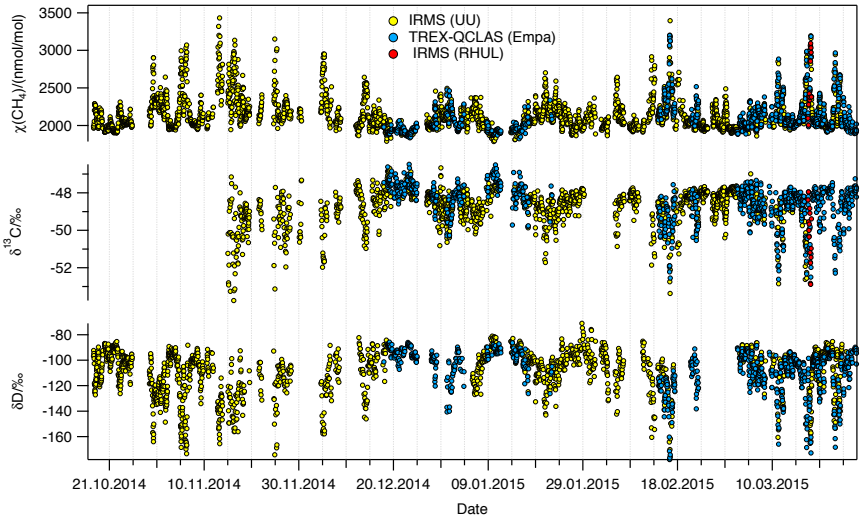


730

731 Fig. 2: $CH_4$ mole fraction, $\chi(CH_4)$, and isotopic composition ($\delta^{13}C$, $\delta D$) measured
732 at the Cabauw tall tower from 17 October 2014 until 29 March 2015. Real-time
733 measurements by IRMS (Utrecht University) are indicated in yellow, TREX-
734 QCLAS (Empa) data in blue. In addition, bag-samples were collected on 17-18
735 March 2015 and analyzed with IRMS in the RHUL laboratory (red circles).

736

Atmos. Chem. Phys. Discuss., doi:10.5194/acp-2016-60, 2016
Manuscript under review for journal Atmos. Chem. Phys.
Published: 10 February 2016


Atmospheric Chemistry and Physics Discussions

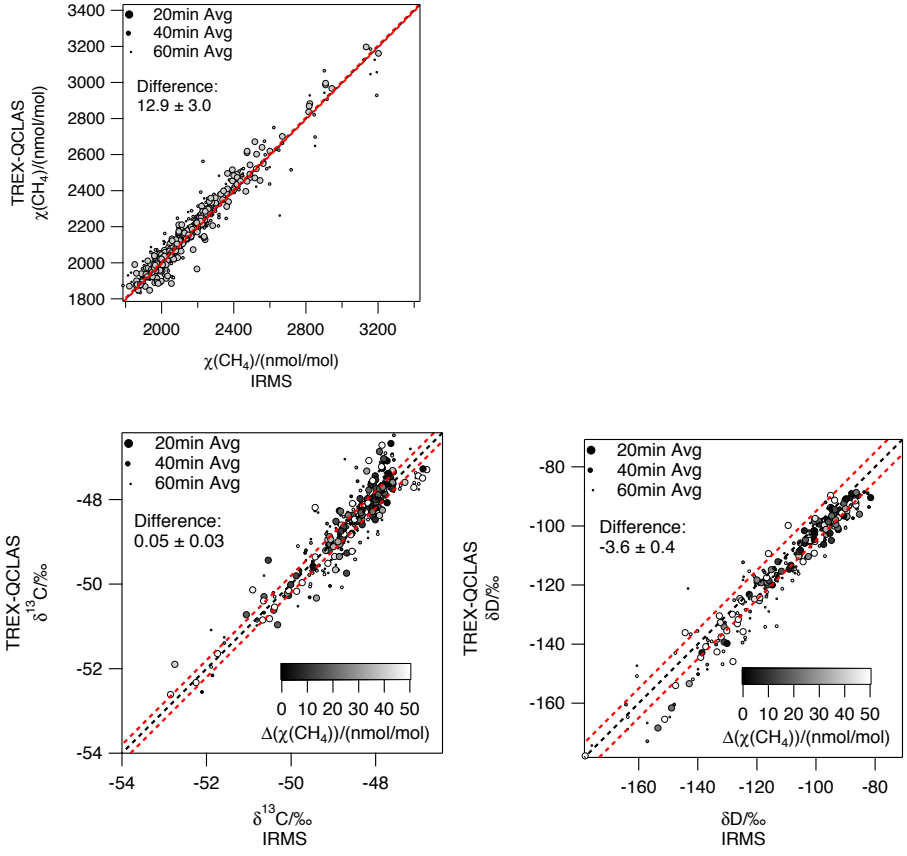


Fig. 3: Correlation diagrams for $CH_4$ mole fraction, $\delta^{13}C$ and $\delta D$ analyzed with IRMS (Utrecht University) and TREX-QCLAS (Empa). The dashed black lines are 1:1 lines, dashed red lines mark the extended WMO compatibility goals of ± 5 nmol/mol, ± 0.2 ‰ and ± 5 ‰ for $CH_4$ mole fraction, $\delta^{13}C$ and $\delta D$, respectively. The temporal difference between IRMS and TREX-QCLAS sampling is indicated by the point size (large: 20 min, medium: 40 min, small: 60 min). For $\delta^{13}C$ and $\delta D$ differences in the $CH_4$ mole fraction of the measurements are represented by the shading (black: identical mole fractions, white: 50 nmol/mol difference).

Atmos. Chem. Phys. Discuss., doi:10.5194/acp-2016-60, 2016
Manuscript under review for journal Atmos. Chem. Phys.
Published: 10 February 2016


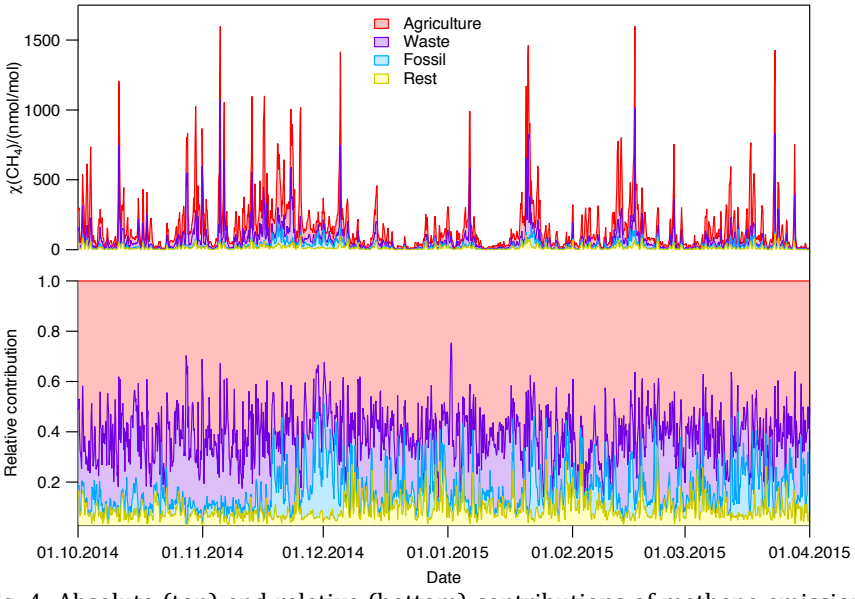


Fig. 4: Absolute (top) and relative (bottom) contributions of methane emissions that are picked up along the 4-day FLEXPART-COSMO trajectories during the campaign. The results shown are from the FLEXPART-COSMO simulations with the TNO-MACC inventory. They indicate major contributions of the following source categories: “agriculture” (mainly ruminants), “waste” (mainly landfills) and “fossil” (fugitive losses from coal, oil and natural gas production and from gas transportation and distribution) to the increase in $CH_4$ mole fractions at Cabauw. The category “rest” primarily represents residential $CH_4$ emissions.

Atmos. Chem. Phys. Discuss., doi:10.5194/acp-2016-60, 2016
Manuscript under review for journal Atmos. Chem. Phys.
Published: 10 February 2016


Atmospheric Chemistry and Physics Discussions

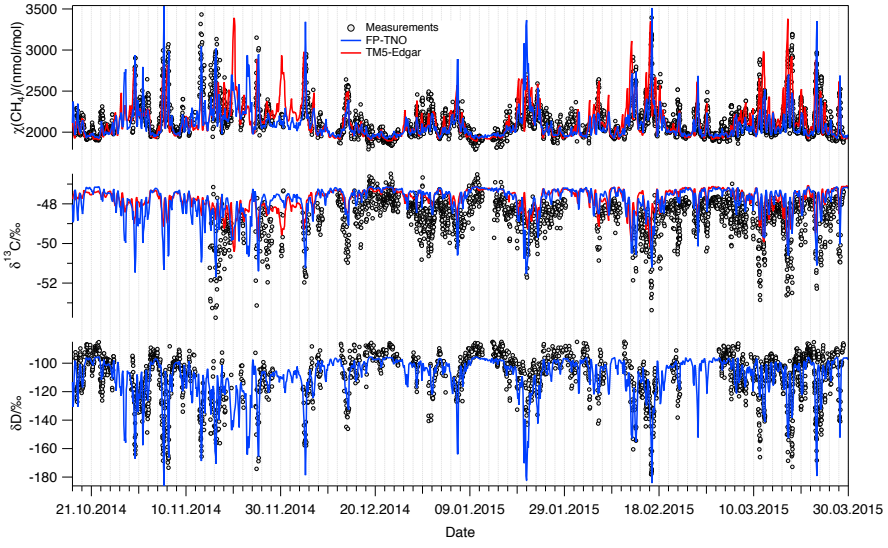


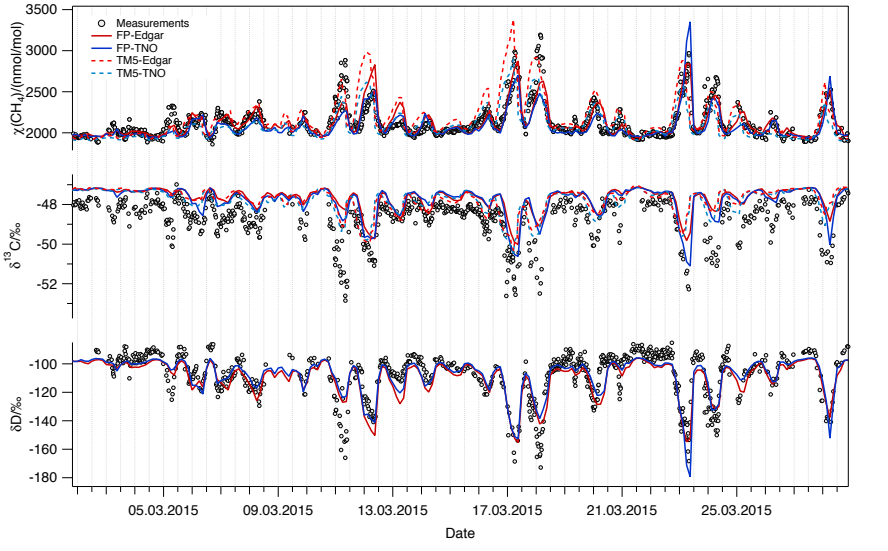


Fig. 5: Comparison of the modeled and measured time series of $CH_4$ mole fraction and isotopic composition ($\delta^{13}C$- and $\delta D$). Measurements are shown as circles and model results as lines. Top graph: two selected model configurations for the entire campaign: FLEXPART-COSMO using the TNO-MACC inventory (blue) and TM5 using the Edgar/Why-Me inventory (red). Bottom graph: Time series for March 2015 with all four model – inventory combinations. For $\delta D$, only the synthetic FLEXPART-COSMO results are available for comparison since TM5 does not simulate $\delta D$.

Atmos. Chem. Phys. Discuss., doi:10.5194/acp-2016-60, 2016
Manuscript under review for journal Atmos. Chem. Phys.
Published: 10 February 2016


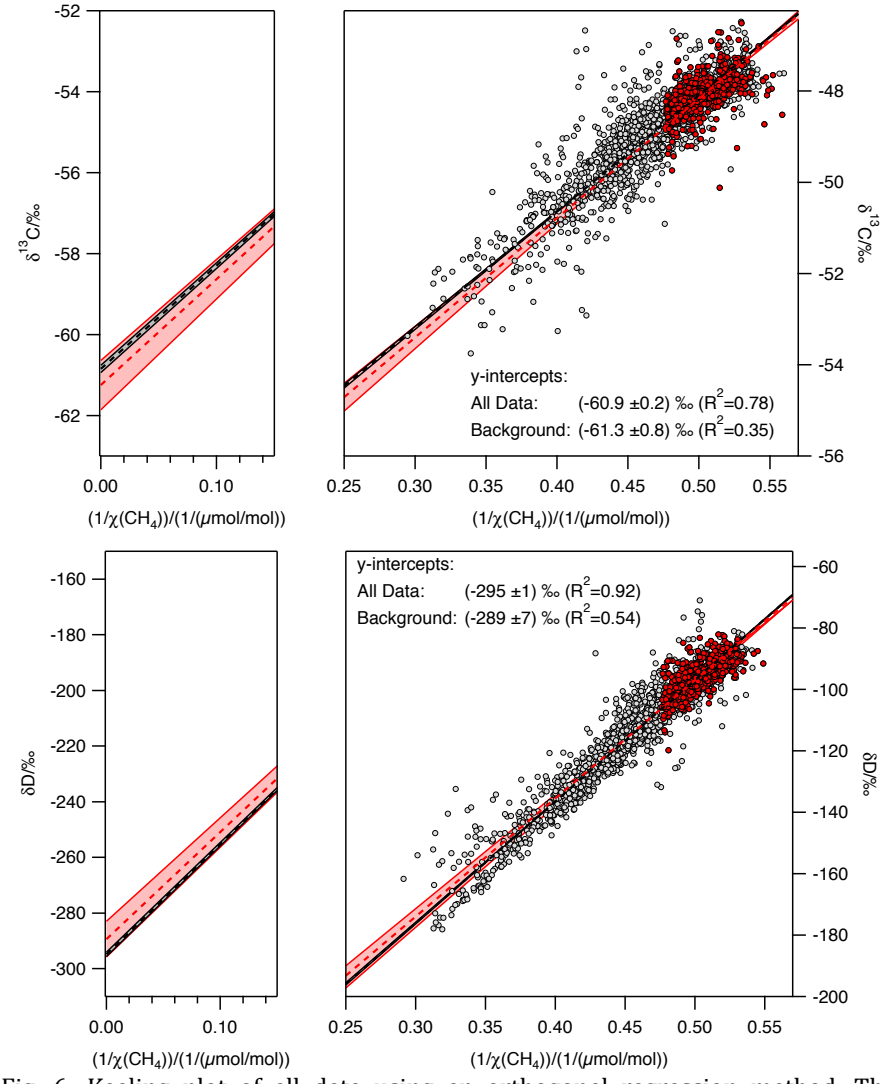


Fig. 6: Keeling plot of all data using an orthogonal regression method. The dashed line indicates the regression line and the shaded area the confidence interval taking into account the measurement uncertainties. The color code indicates all measured data (grey points) and daily background values (red points). Left panels show the region near the y-axis intercept.

Atmos. Chem. Phys. Discuss., doi:10.5194/acp-2016-60, 2016
Manuscript under review for journal Atmos. Chem. Phys.
Published: 10 February 2016


Atmospheric Chemistry and Physics Discussions

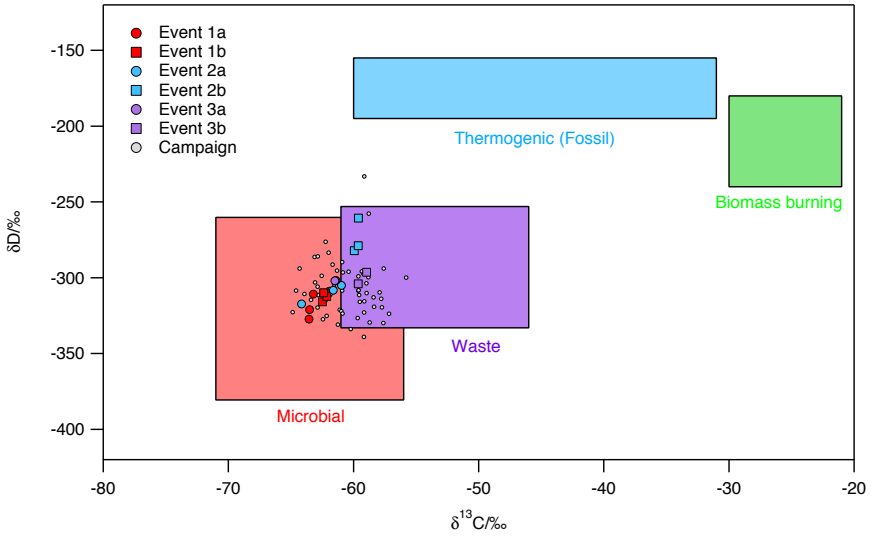


776

777 Fig. 7: MKP intercepts of δD vs. $\delta^{13}C$. The colored areas indicate typical isotope
778 signatures for different source categories. Circles show the 6h-averaged source
779 signatures. Large colored symbols indicate data from the three events that are
780 highlighted in detail in Fig. 9. $\delta^{13}C$ values are taken from table 1 and δD values
781 from recent literature (Rigby et al., 2012).

782

783

Atmos. Chem. Phys. Discuss., doi:10.5194/acp-2016-60, 2016
Manuscript under review for journal Atmos. Chem. Phys.
Published: 10 February 2016


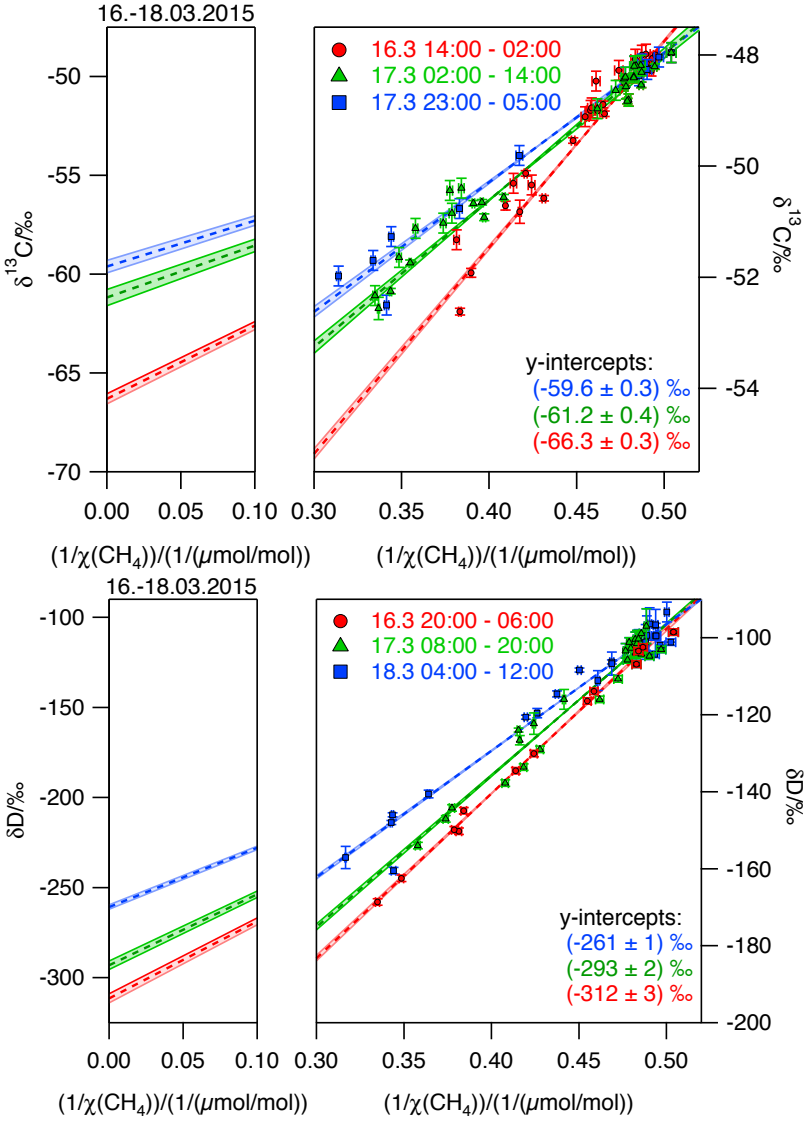


Fig. 8: Keeling plots for the period between 16 and 18 March, illustrating a rapid change in δ values over the course of hours, which is most probably related to a change from mainly ruminant derived $CH_4$ to a significant contribution of fossil and/or waste $CH_4$. The dashed lines indicate the regression line, the shaded areas the uncertainty (one standard deviation) of the regression line. Left panels show the region near the y-axis intercept. Times indicated are Central European Time (CET).

Atmos. Chem. Phys. Discuss., doi:10.5194/acp-2016-60, 2016
Manuscript under review for journal Atmos. Chem. Phys.
Published: 10 February 2016


Atmospheric Chemistry and Physics Discussions

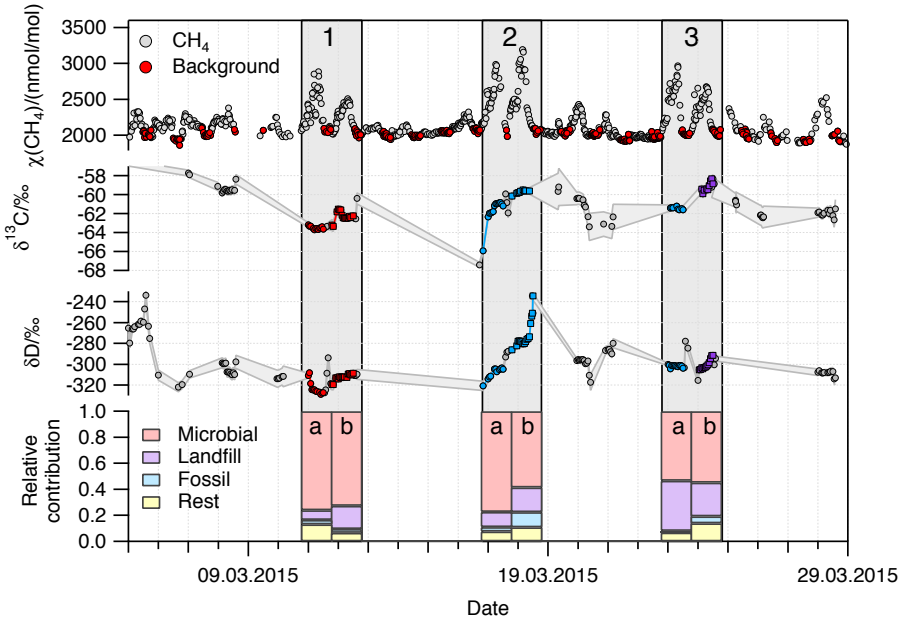


794

795 Fig. 9: Detailed analysis of three 2-day periods with large $CH_4$ elevations in
796 March 2015. The top panel exhibits $CH_4$ mole fraction (grey) with background
797 values in red (10:00-18:00, >2100 nmol/mol). The middle panels show the
798 isotopic source signatures ($\delta^{13}C$, $\delta D$) derived with the 12-h MKP method. The
799 color-coding in the middle panels (red, light blue, purple) indicates characteristic
800 contributions from different sources; red-microbial, light blue-fossil, purple-
801 waste. For consistency, the same color-coding was chosen in Figure 7. The
802 bottom graph presents $CH_4$ source contributions as computed with the
803 FLEXPART-COSMO model using the TNO-MACC inventory, averaged over 24
804 hours.

Atmos. Chem. Phys. Discuss., doi:10.5194/acp-2016-60, 2016
Manuscript under review for journal Atmos. Chem. Phys.
Published: 10 February 2016


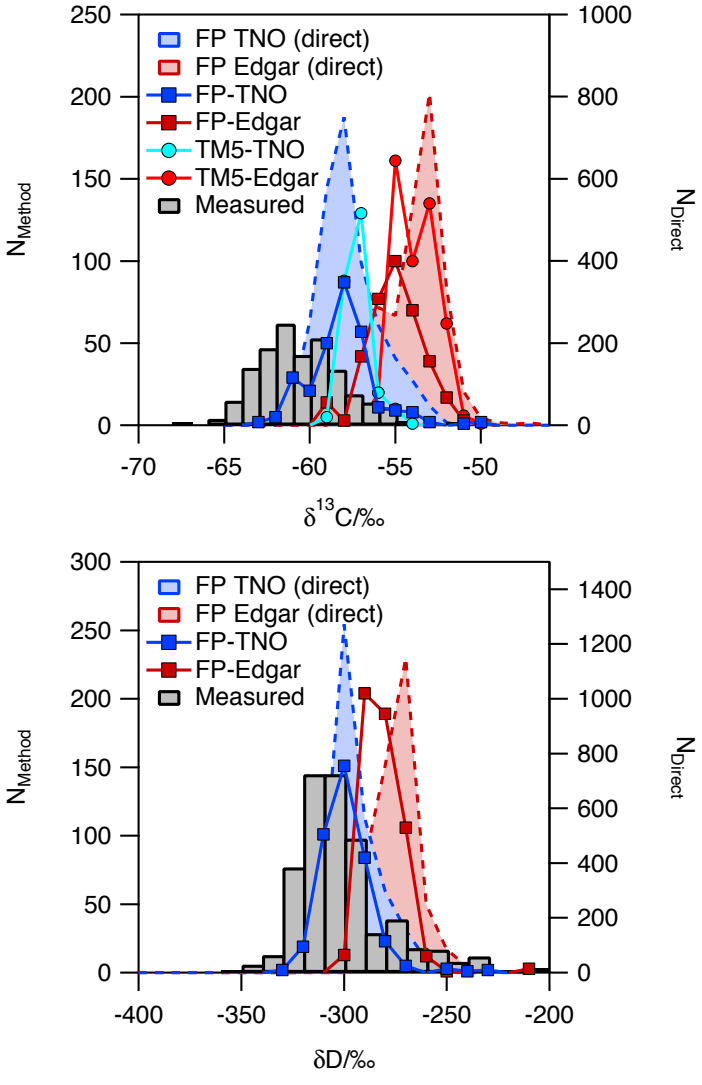


Fig. 10: Histograms of $CH_4$ isotope source signatures at the CESAR site between October 2014 and March 2015. Bin widths are 1 ‰ for $\delta^{13}C$ and 10 ‰ for δD. Source signatures are derived from measured data (grey bins), FLEXPART-COSMO modeling (squares) as well as TM5 modeling (circles) using the 12 h MKP method. Two different inventories, TNO-MACC (blue) and Edgar/LPJ-Why-Me (red), were used. The shaded areas show histograms for the "direct" source signatures that were picked up along the FLEXPART-COSMO trajectory (right axis).

Atmos. Chem. Phys. Discuss., doi:10.5194/acp-2016-60, 2016
Manuscript under review for journal Atmos. Chem. Phys.
Published: 10 February 2016


Atmospheric Chemistry and Physics Discussions

## References

Baertschi, P.: Absolute 18O content of Standard Mean Ocean Water, Earth Planet. Sci. Lett., 31, 341-344, 1976.

Baldauf, M., Seifert, A., Förstner, J., Majewski, D., Raschendorfer, M., and Reinhardt, T.: Operational Convective-Scale Numerical Weather Prediction with the COSMO Model: Description and Sensitivities, Monthly Weather Review, 139, 3887–3905, doi:3810.1175/MWR-D-3810-05013.05011, 2011.

Beck, V., Chen, H. L., Gerbig, C., Bergamaschi, P., Bruhwiler, L., Houweling, S., Röckmann, T., Kolle, O., Steinbach, J., Koch, T., Sapart, C. J., van der Veen, C., Frankenberg, C., Andreae, M. O., Artaxo, P., Longo, K. M., and Wofsy, S. C.: Methane airborne measurements and comparison to global models during BARCA, J. Geophys. Res., 117, D15310, doi:15310.11029/12011JD017345, 2012.

Bergamaschi, P., Brenninkmeijer, C. A. M., Hahn, M., Röckmann, T., Scharffe, D. H., Crutzen, P. J., Elansky, N. F., Belikov, I. B., Trivett, N. B. A., and Worthy, D. E. J.: Isotope analysis based source identification for atmospheric $CH_4$ and CO across Russia using the Trans-Siberian railroad, J. Geophys. Res., 103, D7, 8227-8235, DOI: 8210.1029/8297JD03738, 1998a.

Bergamaschi, P., Houweling, S., Segers, A., Krol, M., Frankenberg, C., Scheepmaker, R. A., Dlugokencky, E., Wofsy, S. C., Kort, E. A., Sweeney, C., Schuck, T., Brenninkmeijer, C., Chen, H., Beck, V., and Gerbig, C.: Atmospheric $CH_4$ in the first decade of the 21st century: Inverse modeling analysis using SCIAMACHY satellite retrievals and NOAA surface measurements, J Geophys Res-Atmos, 118, 7350–7369, doi:7310.1002/jgrd.50480, 2013.

Bergamaschi, P., Lubina, C., Konigstedt, R., Fischer, H., Veltkamp, A. C., and Zwaagstra, O.: Stable isotopic signatures ($\delta^{13}C$, $\delta D$) of methane from European landfill sites, J. Geophys. Res., 103, 8251-8265, doi 8210.1029/8298jd00105, 1998b.

Bergamaschi, P., Schupp, M., and Harris, G. W.: High-precision direct measurements of $^{13}CH_4/^{12}CH_4$ and $CH_3D/^{12}CH_4$ ratios in atmospheric methane sources by means of a long-path tunable diode laser absorbtion spectrometer, Appl. Opt., 33, No.33, 7704-7716, 1994.

Bock, M., Schmitt, J., Behrens, M., Moller, L., Schneider, R., Sapart, C., and Fischer, H.: A gas chromatography/pyrolysis/isotope ratio mass spectrometry system for high-precision $\delta D$ measurements of atmospheric methane extracted from ice cores, Rap. Commun. Mass Spectrom., 24, 621-633, 2010.

Brass, M. and Röckmann, T.: Continuous-flow isotope ratio mass spectrometry method for carbon and hydrogen isotope measurements on atmospheric methane, Atmos. Meas. Tech., 3, 1707-1721, 2010.

Brenninkmeijer, C. A. M., Lowe, D. C., Manning, M. R., Sparks, R. J., and Velthoven, P. F. J. v.: The $^{13}C$, $^{14}C$, and $^{18}O$ isotopic composition of CO, $CH_4$ and $CO_2$ in the higher southern latitudes lower stratosphere, J. Geophys. Res., 100, 26,163-126,172, 1995.

Bruhwiler, L., Dlugokencky, E., Masarie, K., Ishizawa, M., Andrews, A., Miller, J., Sweeney, C., Tans, P., and Worthy, D.: CarbonTracker-$CH_4$: an assimilation system for estimating emissions of atmospheric methane, Atmos. Chem. Phys., 14, 8269-8293, 2014.

Atmos. Chem. Phys. Discuss., doi:10.5194/acp-2016-60, 2016
Manuscript under review for journal Atmos. Chem. Phys.
Published: 10 February 2016




860 Craig, H.: Isotopic standards for carbon and oxygen and correction factors for
861 mass-spectrometric analysis of carbon dioxide, Geochim. Cosmochim. Acta, 12, 133-
862 149, 1957.
863 Dee, D. P., Uppala, S. M., Simmons, A. J., Berrisford, P., Poli, P., and al., e.: The
864 ERA-Interim reanalysis: configuration and performance of the data assimilation
865 system, Quart. J. Roy. Meteor. Soc., 553-579, 2011.
866 Dlugokencky, E. J., Bruhwiler, L., White, J. W. C., Emmons, L. K., Novelli, P.
867 C., Montzka, S. A., Masarie, K. A., Lang, P. M., Crotwell, A. M., Miller, J. B., and
868 Gatti, L. V.: Observational constraints on recent increases in the atmospheric $CH_4$
869 burden, Geophys. Res. Lett., 36, L18803, doi 18810.11029/12009gl039780, 2009.
870 Dlugokencky, E. J., Dutton, E. G., Novelli, P. C., Tans, P. P., Masarie, K. A.,
871 Lantz, K. O., and Madronich, S.: Changes in $CH_4$ and CO growth rates after the
872 eruption of Mt. Pinatubo and their link with changes in tropical tropospheric UV flux,
873 Geophys. Res. Lett., 23, 2761-2764, 1996.
874 Dlugokencky, E. J., Masarie, K. A., Lang, P. M., and Tans, P. P.: Continuing
875 decline in the growth rate of the atmospheric methane burden, Nature, 393, 447-450,
876 1998.
877 Dlugokencky, E. J., Myers, R. C., Lang, P. M., Masarie, K. A., Crotwell, A. M.,
878 Thoning, K. W., Hall, B. D., Elkins, J. W., and Steele, L. P.: Conversion of NOAA
879 atmospheric dry air $CH_4$ mole fractions to a gravimetrically prepared standard scale, J.
880 Geophys. Res., 110, D18306, Doi 18310.11029/12005jd006035, 2005.
881 EDGAR: European Commission, Joint Research Centre (JRC)/Netherlands
882 Environmental Assessment Agency (PBL). , Emission Database for Global
883 Atmospheric Research (EDGAR), Version 4.2. , 2010. Available at
884 http://edgar.jrc.ec.europa.eu., 2010.
885 EDGAR: European Commission, Joint Research Centre (JRC)/Netherlands
886 Environmental Assessment Agency (PBL). Emission Database for Global
887 Atmospheric Research (EDGAR), release version 4.2.
888 http://edgar.jrc.ec.europe.eu., 2009.
889 Etheridge, D. M., Steele, L. P., Francey, R. J., and Langenfelds, R. L.:
890 Atmospheric methane between 1000 AD and present: Evidence of antropogenic
891 emissions and climatic variability, J. Geophys. Res., 103, 15979-15993, 1998.
892 Etiope, G., Lassey, K. R., Klusman, R. W., and Boschi, E.: Reappraisal of the
893 fossil methane budget and related emission from geologic sources, Geophys. Res.
894 Lett., 35, 2008.
895 Eyer, S. and al, e.: Real-time analysis of $\delta^{13}C$- and $\delta D$-$CH_4$ in ambient air with
896 laser spectroscopy: Method development and first intercomparison results., Atmos.
897 Meas. Tech. Discuss., 8, 8925-8970, 2015.
898 Eyer, S., Stadie, N. P., Borgschulte, A., Emmenegger, L., and Mohn, J.: Methane
899 preconcentration by adsorption: a methodology for materials and conditions selection,
900 Adsorption-Journal of the International Adsorption Society, 20, 657-666, 2014.
901 Ferretti, D., Miller, J., White, J., Etheridge, D., Lassey, K., Lowe, D., Allan, B.,
902 MacFarling, C., Dreier, M., Trudinger, C., and Ommen, T. v.: Unexpected changes to
903 the global methane budget over the past 2000 years, Science, 309, 1714-1717, 2005.
904 Fischer, H., Behrens, M., Bock, M., Richter, U., Schmitt, J., Loulergue, L.,
905 Chappellaz, J., Spahni, R., Blunier, T., Leuenberger, M., and Stocker, T. F.: Changing



boreal methane sources and constant biomass burning during the last termination, Nature, 452, 864-867, 2008.

Gros, V., Brenninkmeijer, C. A. M., Jöckel, P., Kaiser, J., Lowry, D., Nisbet, E. G., O'Brian, P., Röckmann, T., and Warwick, N.: Isotope signatures of trace gas sources. In: Emissions Of Atmospheric Trace Compounds, Granier, C., Artaxo, P., and Reeves, C. E. (Eds.), Advances in Global Change Research, Kluwer Academic Pub., Paris, 2004.

Henne, S., Brunner, D., Oney, B., Leuenberger, M., Eugster, W., Bamberger, I., Meinhardt, F., Steinbacher, M., and Emmenegger, L.: Validation of the Swiss methane emission inventory by atmospheric observations and inverse modelling, Atmos. Chem. Phys. Discuss., 2015. 35417-35484, doi:35410.35194/acpd-35415-35417-32015, 2015.

Hiller, R. V., Bretscher, D., DelSontro, T., Diem, T., Eugster, W., Henneberger, R., Hobi, S., Hodson, E., Imer, D., Kreuzer, M., Künzle, T., Merbold, L., Niklaus, P. A., Rihm, B., Schellenberger, A., Schroth, M. H., Schubert, C. J., Siegrist, H., Stieger, J., Buchmann, N., and Brunner, D.: Anthropogenic and natural methane fluxes in Switzerland synthesized within a spatially explicit inventory, Biogeosciences, 11, 1941-1959, doi:1910.5194/bg-1911-1941-2014, 2014.

Houweling, S., Krol, M., Bergamaschi, P., Frankenberg, C., Dlugokencky, E. J., Morino, I., Notholt, J., Sherlock, V., Wunch, D., Beck, V., Gerbig, C., Chen, H., Kort, E. A., Röckmann, T., and Aben, I.: A multi-year methane inversion using SCIAMACHY, accounting for systematic errors using TCCON measurements, Atmos. Chem. Phys., 14, 3991-4012, 2014.

Houweling, S., van der Werf, G. R., Goldewijk, K. K., Röckmann, T., and Aben, I.: Early anthropogenic $CH_4$ emissions and the variation of $CH_4$ and $^{13}CH_4$ over the last millennium, Global Biogeochem Cy, 22, 2008.

Kawagucci, S., Kobayashi, M., Hattori, S., Yamada, K., Ueno, Y., Takai, K., and Yoshida, N.: Hydrogen isotope systematics among $H_2$-$H_2O$-$CH_4$ during the growth of the hydrogenotrophic methanogen Methanothermobacter thermautotrophicus strain Delta H, Geochim Cosmochim Ac, 142, 601-614, 2014.

Keeling, C. D.: The Concentration and Isotopic Abundances of Carbon Dioxide in Rural and Marine Air, Geochim. Cosmochim. Acta, 24, 277-298, 1961.

Khalil, M. A. K., Butenhoff, C. L., and Rasmussen, R. A.: Atmospheric methane: Trends and cycles of sources and sinks, Environmental Science & Technology, 41, 2131-2137, 2007.

Kirschke, S., Bousquet, P., Ciais, P., Saunois, M., Canadell, J. G., Dlugokencky, E. J., Bergamaschi, P., Bergmann, D., Blake, D. R., Bruhwiler, L., Cameron-Smith, P., Castaldi, S., Chevallier, F., Feng, L., Fraser, A., Heimann, M., Hodson, E. L., Houweling, S., Josse, B., Fraser, P. J., Krummel, P. B., Lamarque, J. F., Langenfelds, R. L., Le Quere, C., Naik, V., O'Doherty, S., Palmer, P. I., Pison, I., Plummer, D., Poulter, B., Prinn, R. G., Rigby, M., Ringeval, B., Santini, M., Schmidt, M., Shindell, D. T., Simpson, I. J., Spahni, R., Steele, L. P., Strode, S. A., Sudo, K., Szopa, S., van der Werf, G. R., Voulgarakis, A., van Weele, M., Weiss, R. F., Williams, J. E., and Zeng, G.: Three decades of global methane sources and sinks, Nat Geosci, 6, 813-823, 2013.

Klevenhusen, F., Bernasconi, S. M., Kreuzer, M., and Soliva, C. R.: Experimental validation of the Intergovernmental Panel on Climate Change default values for



ruminant-derived methane and its carbon-isotope signature, Anim Prod Sci, 50, 159-167, 2010.

Krol, M., Houweling, S., Bregman, B., van den Broek, M., Segers, A., van Velthoven, P., Peters, W., Dentener, F., and Bergamaschi, P.: The two-way nested global chemistry-transport zoom model TM5: algorithm and applications, Atmos. Chem. Phys., 5, 417-432, 2005.

Kuenen, J. J. P., Visschedijk, A. J. H., Jozwicka, M., and van der Gon, H. A. C. D.: TNO-MACC_II emission inventory; a multi-year (2003-2009) consistent high-resolution European emission inventory for air quality modelling, Atmos. Chem. Phys., 14, 10963-10976, 2014.

Lassey, K. R., Lowe, D. C., Brenninkmeijer, C. A. M., and Gomez, A. J.: Atmospheric Methane and its Carbon Isotopes in the Southern Hemnisphere: their Time Series and an Instructive Model, Chemosphere, 26, 95-109, 1993.

Lassey, K. R., Lowe, D. C., and Manning, M. R.: The trend in atmospheric methane $\delta^{13}C$ implications for isotopic constraints on the global methane budget, Global Biogeochem Cy, 14, 41-49, 2000.

Loulergue, L., Schilt, A., Spahni, R., Masson-Delmotte, V., Blunier, T., Lemieux, B., Barnola, J. M., Raynaud, D., Stocker, T. F., and Chappellaz, J.: Orbital and millennial-scale features of atmospheric $CH_4$ over the past 800,000 years, Nature, 453, 383-386, 2008.

Lowe, D. C., Brenninkmeijer, C. A. M., Brailsford, G. W., Lassey, K. R., Gomez, A. J., and Nisbet, E. G.: Concentration and $^{13}C$ Records of Atmospheric Methane in New-Zealand and Antarctica - Evidence for Changes in Methane Sources, J. Geophys. Res., 99, 16913-16925, 1994.

MacFarling Meure, C., Etheridge, D., Trudinger, C., Steele, P., Langenfelds, R., Ommen, T. v., Smith, A., and Elkins, J.: Law Dome $CO_2$, $CH_4$ and $N_2O$ ice core records extended to 2000 years BP Geophys. Res. Lett., 33, L14810, doi:14810.11029/12006GL026152 2006.

Merritt, D. A., Brand, W. A., and Hayes, J. M.: Isotope-ratio-monitoring gas chromatography-mass spectrometry: methods for isotopic calibration, Org. Geochem., 21 No. 6/7, 573-583, 1994.

Merritt, D. A., Hayes, J. M., and Des Marais, D. J.: Carbon isotopic analysis of atmospheric methane by isotope-ratio-monitoring gas chromatography-mass spectrometry, J. Geophys. Res., 100 D, 1317-1326, 1995.

Mohn, J., Guggenheim, C., Tuzson, B., Vollmer, M. K., Toyoda, S., Yoshida, N., and Emmenegger, L.: A liquid nitrogen-free preconcentration unit for measurements of ambient N2O isotopomers by QCLAS, Atmos Meas Tech, 3, 609-618, 2010.

Mohn, J., Tuzson, B., Manninen, A., Yoshida, N., Toyoda, S., Brand, W. A., and Emmenegger, L.: Site selective real-time measurements of atmospheric $N_2O$ isotopomers by laser spectroscopy, Atmos Meas Tech, 5, 1601-1609, 2012.

Monteil, G., Houweling, S., Dlugockenky, E. J., Maenhout, G., Vaughn, B. H., White, J. W. C., and Röckmann, T.: Interpreting methane variations in the past two decades using measurements of $CH_4$ mixing ratio and isotopic composition, Atmos. Chem. Phys., 11, 9141-9153, 2011.

Monteil, G., Houweling, S., Guerlet, S., Schepers, D., Frankenberg, C., Scheepmaker, R., Aben, I., Butz, A., Hasekamp, O., Landgraf, J., Wofsy, S. C., and Röckmann, T.: Intercomparison of 15 months inversions of GOSAT and



SCIAMACHY CH4 retrievals, J. Geophys. Res., 118, 11807-11823, doi:11810.11002/12013JD019760, 2013.

Nisbet, E. G., Dlugokencky, E. J., and Bousquet, P.: Methane on the rise—again, Science, 343, 493-495, 2014.

Pataki, D. E., Ehleringer, J. R., Flanagan, L. B., Yakir, D., Bowling, D. R., Still, C. J., Buchmann, N., Kaplan, J. O., and Berry, J. A.: The application and interpretation of Keeling plots in terrestrial carbon cycle research, Global Biogeochem Cy, 17, 1022, doi:1010.1029/2001GB001850, 2003.

Peltola, O., Hensen, A., Helfter, C., Marchesini, L. B., Bosveld, F. C., van den Bulk, W. C. M., Elbers, J. A., Haapanala, S., Holst, J., Laurila, T., Lindroth, A., Nemitz, E., Röckmann, T., Vermeulen, A. T., and Mammarella, I.: Evaluating the performance of commonly used gas analysers for methane eddy covariance flux measurements: the InGOS inter-comparison field experiment, Biogeosciences, 11, 3163-3186, 2014.

Peltola, O., Hensen, A., Marchesini, L. B., Helfter, C., Bosveld, F. C., van den Bulk, W. C. M., Haapanala, S., van Huissteden, J., Laurila, T., Lindroth, A., Nemitz, E., Röckmann, T., Vermeulen, A. T., and Mammarella, I.: Studying the spatial variability of methane flux with five eddy covariance towers of varying height, Agricultural and Forest Meteorology, 214, 456-472, 2015.

Quay, P., Stutsman, J., Wilbur, D., Snover, A., Dlugokencky, E., and Brown, T.: The isotopic composition of atmospheric methane, Global Biogeochem Cy, 13, 445-461, 1999.

Rasmussen, R. A. and Khalil, M. A. K.: Atmospheric Methane ($CH_4$) - Trends and Seasonal Cycles, J. Geophys. Res., 86, 9826-9832, 1981.

Rigby, M., Manning, A. J., and Prinn, R. G.: The value of high-frequency, high-precision methane isotopologue measurements for source and sink estimation, J. Geophys. Res., 117, 2012.

Röckmann, T., Brass, M., Borchers, R., and Engel, A.: The isotopic composition of methane in the stratosphere: High-altitude balloon sample measurements, Atm. Chem. Phys., 11, 13287-13304, 2011.

Sanderson, M. G.: Biomass of termites and their emissions of methane and carbon dioxide: A global database, Global Biogeochem. Cycles, 10, 543–557, 1996.

Sapart, C. J., Monteil, G., Prokopiou, M., van de Wal, R. S. W., Kaplan, J. O., Sperlich, P., Krumhardt, K. M., van der Veen, C., Houweling, S., Krol, M. C., Blunier, T., Sowers, T., Martinerie, P., Witrant, E., Dahl-Jensen, D., and Röckmann, T.: Natural and anthropogenic variations in methane sources during the past two millennia, Nature, 490, 85-88, 2012.

Sapart, C. J., Veen, C. v. d., Vigano, I., Brass, M., Wal, R. S. W. v. d., Bock, M., Fischer, H., Sowers, T., Buizert, C., Sperlich, P., Blunier, T., Behrens, M., Schmitt, J., Seth, B., and Röckmann, T.: Simultaneous stable isotope analysis of methane and nitrous oxide on ice core samples, Atmos. Meas. Tech., 4, 2607-2618, 2011.

Saueressig, G., Bergamaschi, P., Crowley, J. N., Fischer, H., and Harris, G. W.: D/H kinetic isotope effect in the reaction $CH_4$ + Cl, Geophys. Res. Lett., 23, 3619-3622, 1996.

Saueressig, G., Crowley, J. N., Bergamaschi, P., Brühl, C., Brenninkmeijer, C. A. M., and Fischer, H.: Carbon 13 and D kinetic isotope effects in the reactions of $CH_4$ with $O(^1D)$ and OH: New laboratory measurements and their implications for the



1047 isotopic composition of stratospheric methane, J. Geophys. Res., 106, 23127-23138,
1048 2001.

1049 Schmitt, J., Seth, B., Bock, M., van der Veen, C., Möller, L., Sapart, C. J.,
1050 Prokopiou, M., Sowers, T., Röckmann, T., and Fischer, H.: On the interference of Kr
1051 during carbon isotope analysis of methane using continuous-flow combustion-isotope
1052 ratio mass spectrometry, Atmos. Meas. Tech., 6, 1425-1445, 2013.

1053 Seibert, P. and Frank, A.: Source-receptor matrix calculation with a Lagrangian
1054 particle dispersion model in backward mode, Atmos. Chem. Phys., 4, 51-63, 2004.

1055 Snover, A. K. and Quay, P. D.: Hydrogen and carbon kinetic isotope effects
1056 during soil uptake of atmospheric methane, Global Biogeochem. Cycles, 14, 25-39,
1057 2000.

1058 Spahni, R., Chappellaz, J., Stocker, T. F., Loulergue, L., Hausammann, G.,
1059 Kawamura, K., Flückiger, J., Schwander, J., Raynaud, D., Masson-Delmotte, V., and
1060 Jouzel, J.: Atmospheric Methane and Nitrous Oxide of the Late Pleistocene from
1061 Antarctic Ice Cores, Science, 310, 1317-1321, DOI: 1310.1126/science.1120132,
1062 2005.

1063 Spahni, R., Wania, R., Neef, L., Weele, M. v., Pison, I., Bousquet, P.,
1064 Frankenberg, C., Foster, P. N., Joos, F., Prentice, I. C., and Velthoven, P. v.:
1065 Constraining global methane emissions and uptake by ecosystems, Biogeosciences, 8,
1066 1643–1665, doi:1610.5194/bg-1648-1643-2011., 2011.

1067 Sperlich, P., Buizert, C., Jenk, T. M., Sapart, C. J., Prokopiou, M., Rockmann, T.,
1068 and Blunier, T.: An automated GC-C-GC-IRMS setup to measure palaeoatmospheric
1069 $\delta^{13}C$-$CH_4$, $\delta^{15}N$-$N_2O$ and $\delta^{18}O$-$N_2O$ in one ice core sample, Atmos Meas Tech, 6,
1070 2027-2041, 2013.

1071 Sperlich, P., Uitslag, N. A. M., Richter, J. M., Rothe, M., Geilmann, H., Veen, C.
1072 v., Röckmann, T., Blunier, T., and Brand, W. A.: Development and evaluation of a
1073 suite of isotope reference gases for methane in air, submitted to Atmos. Meas. Tech.
1074 Disc., 2016. 2016.

1075 Stohl, A., Forster, C., Frank, A., Seibert, P., and Wotawa, G.: Technical note: The
1076 Lagrangian particle dispersion model FLEXPART version 6.2, Atmos. Chem. Phys.,
1077 5, 2461-2474, 2005.

1078 Sturm, P., Tuzson, B., Henne, S., and Emmenegger, L.: Tracking isotopic
1079 signatures of $CO_2$ at the high altitude site Jungfraujoch with laser spectroscopy:
1080 analytical improvements and representative results, Atmos. Meas. Tech., 6, 1659-
1081 1671, 2013.

1082 Tarasova, O. A., Brenninkmeijer, C. A. M., Assonov, S. S., Elansky, N. F.,
1083 Röckmann, T., and Brass, M.: Atmospheric $CH_4$ along the Trans-Siberian railroad
1084 (TROICA) and river Ob: Source identification using stable isotope analysis, Atmos.
1085 Environ., 40, 5617-5628, 2006.

1086 Tuzson, B., Henne, S., Brunner, D., Steinbacher, M., Mohn, J., Buchmann, B.,
1087 and Emmenegger, L.: Continuous isotopic composition measurements of tropospheric
1088 CO2 at Jungfraujoch (3580 m a.s.l.), Switzerland: real-time observation of regional
1089 pollution events, Atmos. Chem. Phys., 11, 1685-1696, 2011.

1090 Tuzson, B., Mohn, J., Zeeman, M. J., Werner, R. A., Eugster, W., Zahniser, M.
1091 S., Nelson, D. D., McManus, J. B., and Emmenegger, L.: High precision and
1092 continuous field measurements of $\delta^{13}C$ and $\delta^{18}O$ in carbon dioxide with a cryogen-
1093 free QCLAS, Appl. Phys. B-Lasers and Optics, 92, 451-458, 2008.



1094 Umezawa, T., Aoki, S., Nakazawa, T., and Morimoto, S.: A High-precision
1095 Measurement System for Carbon and Hydrogen Isotopic Ratios of Atmospheric
1096 Methane and Its Application to Air Samples Collected in the Western Pacific Region,
1097 Journal of the Meteorological Society of Japan, 87, 365-379, 2009.

1098 Umezawa, T., Machida, T., Aoki, S., and Nakazawa, T.: Contributions of natural
1099 and anthropogenic sources to atmospheric methane variations over western Siberia
1100 estimated from its carbon and hydrogen isotopes, Global Biogeochem. Cycles, 26,
1101 2012a.

1102 Umezawa, T., Machida, T., Ishijima, K., Matsueda, H., Sawa, Y., Patra, P. K.,
1103 Aoki, S., and Nakazawa, T.: Carbon and hydrogen isotopic ratios of atmospheric
1104 methane in the upper troposphere over the Western Pacific, Atmos. Chem. Phys., 12,
1105 8095-8113, 2012b.

1106 Vermeulen, A. T., Hensen, A., Popa, M. E., van den Bulk, W. C. M., and
1107 Jongejan, P. A. C.: Greenhouse gas observations from Cabauw Tall Tower (1992-
1108 2010), Atmos. Meas. Tech., 4, 617-644, 2011.

1109 Wächter, H., Mohn, J., Tuzson, B., Emmenegger, L., and Sigrist, M. W.:
1110 Determination of $N_2O$ isotopomers with quantum cascade laser based absorption
1111 spectroscopy, Optics Express, 16, 9239-9244, 2008.

1112 WMO: 17th WMO/IAEA Meeting on Carbon Dioxide, Other Greenhouse Gases,
1113 and Related Measurement Techniques (GGMT-2013) 10-13 June 2013, GAW Report
1114 No. 213,, World Meteorological Organization, Geneva, Switzerland, Beijing, China,
1115 2014.

1116 Wolf, B., Merbold, L., Decock, C., Tuzson, B., Harris, E., Six, J., Emmenegger,
1117 L., and Mohn, J.: First on-line isotopic characterization of $N_2O$ above intensively
1118 managed grassland, Biogeosciences, 12, 2517-2531, 2015.

1119 Yamada, K., Ozaki, Y., Nakagawa, F., Tanaka, M., and Yoshida, N.: An
1120 improved method for measurement of the hydrogen isotope ratio of atmospheric
1121 methane and its application to a Japanese urban atmosphere, Atmos. Environ., 37,
1122 1975-1982, 2003.

1123 Zazzeri, G., Lowry, D., Fisher, R. E., France, J. L., Lanoiselle, M., and Nisbet, E.
1124 G.: Plume mapping and isotopic characterisation of anthropogenic methane sources,
1125 Atmos. Environ., 110, 151-162, 2015.

1126